



Faculty of Engineering

**Experimental Investigation of Mixing Performance in Laser-fabricated
Microfluidic Micromixers**

Fahizan Bin Mahmud

**Master of Engineering
2020**

Experimental Investigation of Mixing Performance in Laser-fabricated Microfluidic Micromixers

Fahizan Bin Mahmud

A thesis submitted

In fulfillment of the requirements for the degree of Master of Engineering

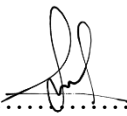
(Mechanical Engineering)

Faculty of Engineering
UNIVERSITI MALAYSIA SARAWAK

2020

DECLARATION

I declare that the work in this thesis was carried out in accordance with the regulations of Universiti Malaysia Sarawak. Except where due acknowledgements have been made, the work is that of the author alone. The thesis has not been accepted for any degree and is not concurrently submitted in candidature of any other degree.



.....

Signature

Name: Fahizan Bin Mahmud

Matric No.: 19020003

Faculty of Engineering

Universiti Malaysia Sarawak

Date: 25 July 2020

ACKNOWLEDGEMENT

Alhamdulillah, all praise to Allah for his blessing for giving me the opportunity to complete this thesis as a requirement for Master of Engineering (Mechanical). I would like to thank to Allah for bringing me through this time, towards the completion of my Master thesis and for countless gifts that have been given to me throughout my life.

Special thanks and appreciation to my supervisor, Dr. Khairul Fikri bin Tamrin for his guidance, encouragement and advice using his knowledge and experience throughout this period. I am so thankful for the compassion and patience shown by him during the whole duration of project and that helped me a lot towards the completion of this thesis.

I would like to express my sincere gratitude to Universiti Malaysia Sarawak (UNIMAS), particularly Department of Mechanical and Manufacturing, Faculty of Engineering UNIMAS for providing the opportunity to undertake the project on “Experimental Investigation of Mixing Performance in Laser-fabricated Microfluidic Micromixers”. I would like to thanks to all Faculty of Engineering staff especially Mr. Mohd. Fairudi Bin Mohd. Jamil, Mr. Mohd Rhyier Juen Abdullah, Mdm. Hasmiza Kontet, Mdm. Siti Fazilah Mohammad and Mr. Ireman Bolhassan for their great help and support.

Greatest thanks to my supportive parents and family for their continuous support, help and prayer throughout this project period. Last but not least, I would like to extend my gratitude to all my friends for their direct and indirect support along the way. I could not express how much gratitude towards them, but I sincerely wishes all of them best for everything, now and for their future.

ABSTRACT

Microfluidic mixing is a key process in miniaturized analytical system. Achieving adequate mixing performance is considerably difficult in micromixer as the flow is always associated with unfavourable laminar flow. The mixing performance of these micromixers are generally characterized as a function of mixing index based on dispersion (homogeneity) information, leading to either overestimated or underestimated mixing index. This research presents a novel method to determine mixing index of micromixers based on red, green and blue (RGB) colour model by decoding mixing images to their respective red, green and blue pixel intensities. The proposed method is foreseen handy and robust in characterizing mixing in real time for gradient mixing in networked microchannels and multivortex mixing for the manipulation of fluids, particles and biological substances. Several digital composite images were used to perform initial benchmarking, and the proposed method accurately quantified the mixing index significantly better than previously adopted methods. T-, Y-, and Dean micromixer were laser fabricated and the proposed Dean micromixer exhibits higher mixing performance (about 27 % better) as compared to T- and Y- micromixers for $40 \leq Re \leq 100$. Extraneously induced ultrasound and thermal energy were studied and their effects towards mixing performance is more significant at $5 \leq Re \leq 20$ because of prolonged mechanical effect within the system. It is also found that the mixing index increases of about 6 % to 10 % at various Reynolds number once the sonicated mixing fluids were heated from 30 °C to 60 °C. The proposed method and improved design of the Dean micromixer are potentially useful for sensitive microfluidic devices as direct contact of the inductive energy sources may cause unwanted substrate damage and structural deformation especially for applications in biological analysis and chemical synthesis.

Keywords: Microfluidic, micromixer, mixing index, ultrasound, thermal energy

Eksperimen Prestasi Pencampuran Dalam Pengadun Mikro yang Direka Dengan Laser

ABSTRAK

*Pengadun bendalir mikro adalah proses utama dalam sistem analisis miniatur. Prestasi pencampuran yang mencukupi merupakan perkara yang sukar untuk diperolehi dalam pengadun mikro kerana aliran bendalir bersifat laminar. Prestasi pencampuran dalam pengadun mikro pada umumnya dicirikan sebagai fungsi indeks pencampuran berdasarkan maklumat penyebaran (keseragaman). Hal ini menyebabkan bacaan indeks pencampuran menjadi kurang tepat. Kajian ini memperkenalkan cara baru untuk menentukan bacaan indeks pencampuran berdasarkan model warna merah, hijau dan biru (RGB) dengan menyahkodkan imej pencampuran kepada intensiti pixel merah, hijau dan biru secara berasingan. Kaedah yang dicadangkan dijangka berguna untuk mencirikan prestasi pencampuran masa nyata untuk pencampuran kecerunan dalam rangkaian saluran mikro, pencampuran pelbagai vortex untuk memanipulasi cecair, zarah dan bahan-bahan biologi. Beberapa imej komposit digital telah digunakan sebagai penanda aras dan kaedah yang dicadangkan berjaya mengukur indeks pencampuran dengan tepat berbanding kaedah-kaedah yang terdahulu. Pengadun mikro T-, Y- dan Dean telah direka dengan laser dan didapati bahawa pengadun mikro Dean menunjukkan prestasi pencampuran yang lebih tinggi (lebih kurang 27 %) berbanding pengadun mikro -T dan -Y untuk bacaan $40 \leq Re \leq 100$. Rangsangan luaran ultrabunyi dan tenaga haba telah dikaji sebagai kaedah untuk meningkatkan indeks pencampuran. Kesan rangsangan-rangsangan ini terhadap prestasi pencampuran adalah lebih ketara pada $5 \leq Re \leq 20$ kerana lanjutan kesan mekanikal dalam sistem tersebut. Indeks pencampuran bendalir yang dirangsang dengan ultrabunyi juga didapati meningkat dari 6 % ke 10 % untuk pelbagai nombor Reynolds apabila suhu dinaikkan dari 30 °C ke 60 °C. **Kaedah yang dicadangkan dan reka bentuk pengadun mikro***

Dean yang lebih baik berpotensi digunakan untuk peranti mikrofluida yang sensitif kerana sumber tenaga induktif secara langsung boleh menyebabkan kerosakan substrat yang tidak diinginkan dan perubahan struktur terutamanya dalam analisis biologi dan sintesis bahan kimia.

Kata kunci: *Bendalir mikro, pengadun mikro, indeks pencampuran, ultrabunyi, tenaga haba*

TABLE OF CONTENTS

	Page
DECLARATION	i
ACKNOWLEDGEMENT	ii
ABSTRACT	iii
<i>ABSTRAK</i>	v
TABLE OF CONTENTS	vii
LIST OF TABLES	xi
LIST OF FIGURES	xii
LIST OF ABBREVIATIONS	xiv
CHAPTER 1: INTRODUCTION	1
1.1 Study Background	1
1.2 Problem Statement	2
1.3 Scope of Study	3
1.4 Hypothesis	4
1.5 Objectives	4
CHAPTER 2: LITERATURE REVIEW	5
2.1 Introduction	5
2.2 Applications of Micromixer	5
2.2.1 Disease Diagnosis	5

2.2.2	Drug Development	6
2.2.3	Biological Analysis	8
2.3	General Overview of Micromixer	9
2.3.1	Active Mixing	11
2.3.2	Passive Mixing	13
2.3.3	Passive Micromixer Designs	18
2.4	Passive Flow Driving Mechanism	28
2.4.1	Surface Tension	28
2.4.2	Capillary Effects	29
2.4.3	Gravity Driven	29
2.5	Characterization of Mixing Performance	30
2.6	Fabrication Method	33
2.6.1	Lithography	33
2.6.2	Laser Micromachining	34
2.6.3	Mechanical Engraving and Milling	36
2.6.4	Casting	37
2.6.5	Wet Etching	38
2.7	Conclusion	38
CHAPTER 3: METHODOLOGY		39
3.1	Introduction	39

3.2	Microfluidic Device Design and Fabrication	40
3.3	Syringe Pump Fabrication	43
3.3.1	Syringe Pump Mechanism	43
3.3.2	Fabricated Syringe Pump	45
3.4	Experimental Setup	47
3.4.1	Methods for Validation of Proposed Mixing Index Quantification	49
3.4.2	Mixing Performance of T-, Y- and Dean Micromixers	50
3.4.3	Extraneously Induced Ultrasound and Thermal Energy	50
3.5	Mixing Index Quantification	50
3.5.1	Theory of the Proposed Method	51
3.5.2	Sensitivity Enhancement for the Proposed Method	53
3.5.3	RGB Values After Sensitivity Enhancement	55
	CHAPTER 4: RESULTS AND DISCUSSION	58
4.1	Validation of Proposed Method using Digital Composite Images	58
4.2	Benchmarking Against Other Methods using T- and Y-Micromixers	60
4.3	Comparison of Mixing Index Between T-, Y- and Dean Micromixers	64
4.4	Influence of Extraneously Induced Ultrasound and Thermal Energy on Mixing	67
	CHAPTER 5: CONCLUSION AND RECOMMENDATIONS	71
5.1	Conclusion	71
5.2	Recommendations	72

REFERENCES

73

APPENDICES

86

LIST OF TABLES

		Page
Table 2.1	Summary of Mixing Mechanisms	17
Table 2.2	Summary of Key Findings for Mixing Enhancement in Passive Micromixers	25
Table 3.1	Stepper Motor Speed for Specific Reynolds Number	47
Table 3.2	Sets of Reference RGB Values for Blue, Yellow and Green Solutions	57
Table 4.1	Benchmarking Against Different Mixing Index Calculation Methods Using Digital Composite Images	59
Table 4.2	Actual Mixing Images in T-Micromixer at Different Reynolds Numbers	60
Table 4.3	Actual Mixing Images in Y-Micromixer at Different Reynolds Numbers	61
Table 4.4	Actual Mixing Images in Dean Micromixer at Different Reynolds Numbers	65
Table 4.5	Actual Mixing Images in Dean Micromixer for 40 kHz Ultrasound and 30 °C at Different Reynolds Numbers	68
Table 4.6	Actual Mixing Images in Dean Micromixer for 40 kHz Ultrasound and 60 °C at Different Reynolds Numbers	68

LIST OF FIGURES

	Page
Figure 2.1 An Overview of Mixing and Flow Driving Mechanism of Micromixer	10
Figure 2.2 Geometrical Configuration of Unbalanced Splits and Collisions Microfluidic Device	19
Figure 2.3 Different Geometrical Configuration Used in This Study (Units in mm)	22
Figure 2.4 Configuration of SeLMA Micromixer	23
Figure 2.5 Top View of Different Designs of Microfluidic Devices	24
Figure 2.6 Fabrication Methods of Microfluidic Devices	33
Figure 3.1 Methodology for Micromixers Investigation	39
Figure 3.2 Micromixer Designs and Measurement Points (Position A and B)	40
Figure 3.3 Schematic Diagram of the Fabrication Procedure for T-Micromixer	42
Figure 3.4 Fabricated T-, Y-, and Dean Micromixer	42
Figure 3.5 Leak Test on T-Micromixer Using Blue Dye	43
Figure 3.6 Syringe Pump Mechanism	44
Figure 3.7 Fabricated Syringe Pump	45
Figure 3.8 Wiring Arrangement for A4988 Motor Driver Connected to Arduino UNO	46

Figure 3.9	Schematic Diagram of the Micromixing Experiment	48
Figure 3.10	Experimental Setup of the Micromixing Experiment	49
Figure 3.11	Mixing of Three Dissimilar Fluids Coming from Three Separate Inlets	52
Figure 3.12	Overview of the Proposed Method	53
Figure 3.13	Illustration of Transitional Region	54
Figure 3.14	Effects of Sensitivity Enhancement on Calculated Mixing Index	55
Figure 3.15	RGB Values of Premixed Green Solution at Different Concentration Levels	56
Figure 3.16	Effect of Sensitivity Enhancement on Detecting the Transitional Region	57
Figure 4.1	Mixing Index of T- and Y-Micromixers at Position B Calculated Using the Proposed Method	62
Figure 4.2	Comparison of Calculated Mixing Index in T-Micromixer Against Other Methods	63
Figure 4.3	Comparison of Calculated Mixing Index in Y-Micromixer Against Other Methods	64
Figure 4.4	Mixing Index of T-, Y- and Dean Micromixer at Position B	66
Figure 4.5	Mixing Index of Dean Micromixer for Different Operating Conditions at Position B	70

LIST OF ABBREVIATIONS

CKD	Chronic kidney disease
CMYK	Cyan, magenta, yellow, key
CNC	Computer numerical control
CTCs	Circulating tumour cells
HSI	Hue, saturation, intensity
LoC	Lab-on-chip
MI	Mixing Index
PCR	Polymerase chain reaction
PDMS	Polydimethylsiloxane
PMA	Propidium monoazide
PMMA	Poly(methyl methacrylate)
PoC	Point of care
RGB	Red, green, blue
SeLMA	Sequential logarithmic mixing apparatus
SESM	Stacking E-shape micromixer
SHM	Staggered herringbone mixer
STB	Shifted trapezoidal blade
YCSAR	Y-shaped circle split and recombination
YRCSAR	Y-shaped rhombus-circle split and recombination
YRSAR	Y-shaped rhombus split and recombination

CHAPTER 1

INTRODUCTION

1.1 Study Background

Microfluidics is an emerging field in which fluid behaviours at micro scale are studied. For the past few decades, microfluidic system has become a major topic of research due to their widespread application especially in several areas such as biomedical diagnostics, chemical analysis, drug development, precipitation and food industry (Lee et al., 2016) to name a few. The miniaturized characteristics of microfluidic devices has led to substantial cost reduction since they use minimum amount of chemical reagents and simultaneously reduce overall process waste (Ward & Fan, 2015). In addition, noticeable increase in surface area to volume ratio will substantially reduce the sample volume and reagent consumption, increase throughput, minimize operation complexity and maximize information extracted (Sivashankar et al., 2016).

Homogenous and rapid micromixing are important criteria for the abovementioned applications since micromixer serves as a crucial component of many functional microfluidic devices. Attaining sufficient mixing performance is considerably difficult as the flow is typically laminar, and mixing is dominated by molecular diffusion which is slow and ineffective (Fu et al., 2017; Ward & Fan, 2015). Fluid flow inside microfluidics is highly laminar ($Re < 100$) due to the dominant viscous effect over inertial forces within the flow. Slow mixing rate between the reactants has become a critical challenge in this field and various types of mixer configurations and designs have been proposed to tackle this issue (You et al., 2015). For this reason, enhancement of micromixing through active and/or passive approaches is necessary. Active mixing mechanism depends on provision of external

energy, for example, by means of micro-stirrer, heat, magnetohydrodynamic and ultrasound. On the other hand, passive mixing mechanism depends on manipulation of microchannel geometry to increase contact surface area and residence time between mixing fluids.

1.2 Problem Statement

The mixing performance of micromixers are generally characterized as a function of mixing index. On the basis of colour changes, several quantitative mixing indices have been defined based on intensity images recorded using typical digital video microscopes (Ansari et al., 2010; Le The et al., 2015; Nimafar et al., 2012; Wang et al., 2018). The digitally captured intensity images are usually stored in the format of three 8-bit monochromatic red, green and blue colours (RGB), which can be converted to the grayscale, Cyan/Magenta/Yellow/Key (CMYK) or Hue/Saturation/Intensity (HSI) colour model. The mixing index can be calculated using grayscale images as described in (Chen et al., 2016b; Le The et al., 2015; Nimafar et al., 2012; Wang et al., 2018). The main limitation is that the expected normalized pixel intensity is considered constant which is not entirely accurate in practice. To incorporate varying normalized pixel intensity in to the calculation of mixing index, another method was proposed for HSI images by (Chen & Wang, 2015; Fu et al., 2017; Johnson et al., 2002; Sivashankar et al., 2016). Meanwhile, to accommodate frame-varying mean intensity in to the calculation of mixing index, the third method was proposed by (Engler et al., 2004; Fu et al., 2017; Luo et al., 2006; Parsa et al., 2014; Rafeie et al., 2017; Shah et al., 2019). The three abovementioned methods are essentially based on dispersion (homogeneity) information of the intensity images. One common and clear limitation is that the individual RGB values are first averaged before mixing index is computed. This could lead to overestimating or underestimating of the calculated mixing index.

Although passive mixing is preferable due to simple mixing principle, their mixing performance is lower and difficult to control compared to active micromixer (Ward & Fan, 2015). Active micromixers utilizing ultrasound and thermal energy have been demonstrated effective to enhance micromixing process, however, integration of these energy source within the devices is a non-trivial task (Xu et al., 2011; Yang et al., 2001; Yaralioglu et al., 2004). In addition, direct contact of the energy sources may cause substrate damage and structural deformation (Parvizian et al., 2011).

1.3 Scope of Study

This research covers the area of micromixing as a fundamental process inside microfluidics system. The scopes of this study are:

- i. Design and laser fabrication of T-, Y- and Dean micromixers using CO₂ laser.
- ii. Development and benchmarking of the proposed mixing index quantification method utilising RGB model with three different methods from literature.
- iii. Comparison of mixing performance of two dissimilar coloured liquids inside T-, Y- and Dean micromixers in the range of $5 \leq Re \leq 100$.
- iv. Comparison and evaluation of mixing performance inside the Dean micromixer ($5 \leq Re \leq 100$) in three different operating conditions: room temperature (25 °C), 40 kHz ultrasonic vibration at 30 °C and 40 kHz ultrasonic vibration at 60 °C.

1.4 Hypothesis

- i. Low Reynolds number could cause the mixing fluid to spend more time inside the microchannel. This longer time interval (residence time) between entry and exit of the fluid are predicted to increase molecular diffusion between the mixing fluids throughout the microchannel.
- ii. Theoretically, the effects of Dean vortices inside a curved microchannel is directly proportional to the Reynolds number. Increasing the Reynolds number are expected to affect the mixing performance of the Dean micromixer due to enhanced Dean vortices.
- iii. Extraneously induced ultrasound and thermal energy may generate disturbance inside the microchannel and reduce the fluid viscosity, respectively. The prolonged disturbance inside the microfluidic system are predicted to help in enhancing the micromixing process.

1.5 Objectives

The main objectives of this research are:

- i. To design and laser-fabricate T-, Y- and Dean micromixers.
- ii. To compare performance of T-, Y- and Dean micromixers at varying Reynolds number using novel method of mixing index quantification based on RGB colour model.
- iii. To investigate the effect of extraneously induced ultrasound and thermal energy towards mixing performance of Dean micromixer.

CHAPTER 2

LITERATURE REVIEW

2.1 Introduction

Microfluidics has become an interesting topic due to its widespread application in healthcare, drug development, biological analysis, chemical and biomedical analysis, food processing, pharmaceutical, pathogen detection and others. The miniaturized characteristics of microfluidic devices lead to substantial cost reduction in which these devices use minimum amount of samples, chemical reagents and reduce overall waste generated (Ward & Fan, 2015). In particular, micromixer serves as a crucial component of many functional microfluidic devices. Fluid flow inside microfluidics is highly laminar ($Re < 100$) due to the dominant viscous effect over inertial forces within the flow. Therefore, the mixing process inside the micromixer depend almost entirely on diffusion, which is slow and ineffective (Le The et al., 2015). Slow mixing rate between the reactants has become a critical challenge in this field and various types of mixer configurations and designs have been proposed to tackle this issue (You et al., 2015). This chapter focuses relevant methods that have been developed in the past to increase the efficiency of micromixers without compromising the integrity of the devices. The following section provides an overview of the selected applications of micromixers in disease diagnosis, drug development and biological analysis.

2.2 Applications of Micromixer

2.2.1 Disease Diagnosis

Potential growth of microfluidic technologies in medicine and healthcare are limitless. The nature of Lab-on-Chip (LoC) which can perform rapid, economical, ease-of-

operation and reliable diagnosis are the key factors for the increased demand of these devices. LoC-based point of care (PoC) system has been employed for chronic disease diagnosis due to these aforementioned key factors (Wu et al., 2018). According to World Health Organization (2018), it was estimated that 1.6 million of death in 2016 were directly related to diabetes, and almost half of the death was associated with high glucose level for people below age of 70. Although many blood glucose meters are commercially available in the market, the accuracy of these devices remain low (Evans et al., 2014; Wu et al., 2018). For this reason, a number of microfluidic paper-based analytical devices have been developed to improve the diagnosis efficiency and control multiple reagents and analytes simultaneously. In addition to improved efficiency in detecting glucose level, LoC are also reliable in detecting uric acid, nitrite and bovine serum albumin (De Tarso Garcia et al., 2014).

In addition, LoC was proven as a convenience means for early detection of chronic kidney disease (CKD). The most common methods to detect CKD is by measuring creatinine (waste products when it breaks up) concentration level in blood (Wu et al., 2018). However, conventional clinical measurement of the creatinine concentration level requires high-end and expensive equipment. LoC device to measure the level of creatinine has been developed for screening purposes incorporating electrophoretic separation and conductivity detection (Ávila et al., 2013).

2.2.2 Drug Development

Different drug development processes require different configurations of microfluidic devices. For instance, merging microchannels such as T- and Y- micromixers can be utilized to ensure mixing of various reactants with varying concentrations. These

reactants can be analysed up to micro-scale level. Microfluidic devices provide a higher level of control to manipulate concentration and flow characteristics during the mixing process. Therefore, this level of control over the fluids will lead to useful extraction of data required especially in drug discovery and development. Kastner et al. (2015) proposed a new method utilizing micromixer to prepare liposomal solubilising systems. This is because liposomes have the capability to act as solubilizing agent for drugs that has low aqueous solubility. Current liposome solubilising technology lacks the scalability and typically needs high-cost production methods. In short, it has the capability to replace conventional methods of liposomes preparation.

Jia et al. (2016) used micromixer to increase reaction and production of antitumor drugs, taking advantage of liposomes as carriers for drug delivery due to biocompatibility and good release properties. Jia et al. (2016) discovered that the utilization of micromixer results in lower compound consumption and high efficiency in comparison with conventional methods. Apart from liposomes, polymeric nanoparticles are also considered as excellent drug carriers which demonstrated increased stability of drugs and control over their release properties in nanoprecipitation (Ding et al., 2016). The main requirement for this is the fast mixing of polymers solution with specific solvents until they are completely miscible. Since microfluidic devices have the capability to manipulate fluid flow at microscale level, they are the most suitable tool to control solvent transfer in nanoprecipitation. Accordingly, drug-loaded polymer can be effortlessly produced by nanoprecipitation of a polymer using specific drugs with the help of microfluidic devices. Ding et al. (2016) noted that micromixers yield a high efficiency in term of controlled mixing between the reagents especially in nanoprecipitation process.

Kim et al. (2012) developed a programmable microfluidic culture array with 64 individual cell culture chambers for drug candidate screening purposes. The design was based on the concept of simple diffusive micromixer for generation of the desired drug combination. The developed microfluidic device was used to optimize combination of multiple drugs for treatment of PC3 prostate cancer cells. Furthermore, the developed system was also capable of finding the optimum drug combination for other diseases, not only limited to PC3 prostate cancer cells (Kim et al., 2012).

2.2.3 Biological Analysis

Compared to traditional methods that used culture of single media which is inherently time consuming, expensive and requiring large sample volume, microfluidic system was proven capable processing multiple samples with smaller reagent volume with less time using a single device (Lee & Fu, 2018). Wang et al. (2013) used the concept of unbalanced splits and collisions in micromixer for rapid detection of bacteria cells. *Escherichia coli* (*E. coli*) sample was tagged with fluorescent dye in order to measure concentration of this bacteria at the preconcentrated region. The developed device can be easily fabricated and integrated with handheld device system for real time detection of bacteria by concentrating them at a target position for imaging purposes.

Duarte-Guevara et al. (2016) performed Propidium monoazide (PMA) labelling on microfluidic device for detection of *Salmonella Typhi* (*S. Typhi*) and *E. coli*. PMA is a molecule that covalently bonds to DNA when exposed to light which allows detection of these two groups of bacteria. Three labelling stages which comprise of mixing, incubation and cross-linking were performed in a single microfluidic device, leading to a simpler and faster process compared to standard procedure. Furthermore, the cost for the whole process

was significantly reduced as it only consumed 5 % of the reagents required in standard procedure (Duarte-Guevara et al., 2016). The presented labelling method demonstrated high sensitivity and specificity comparable to that of standard procedure.

Circulating tumour cells (CTCs) are primary tumour cells moving through blood circulation which are responsible for metastatic disease. Since the size of CTC is similar to leucocytes, CTCs always found to be missing during isolation process. Considering the significance of preventing any loss of CTCs during isolation process, Lin et al. (2013) developed a microfluidic device that continuously coat the cell with microbeads. The coating process was done by generating secondary vortex flow perpendicular to the main flow which results in CTCs size amplification. The proposed coating process utilizing micromixing was able to accurately isolate CTCs from human blood sample during filtration. This was demonstrated effective for isolating two types of breast cancer cells namely, EpCAM-positive and EpCAM-negative.

2.3 General Overview of Micromixer

Micromixers are one of the important components in microfluidic devices that are used in wide range of applications. Since the channels are small in features, sizes and geometries, there are number of dimensionless parameters that can be used to characterize fluid flow in microchannels such as Reynolds number, Peclet number, Schmidt number, Dean number and Poiseuille number. These dimensionless numbers are predominantly governed by viscous effect in the absence of turbulent fluctuations in these systems (Ta et al., 2015), placing a challenge for researcher to address low mixing efficiency in this laminar regime since mixing depends solely on molecular diffusion (Ta et al., 2015; You et al., 2015).

Therefore, a number of studies have been conducted to design an effective micromixer that can increase mixing efficiency.

Figure 2.1 shows an overview of mixing and flow driving mechanism of micromixers. Generally, the mixing mechanism can be divided into two mixing principles, namely active and passive mixing. Flow driving mechanisms that will be used to initiate the flow inside the system can be also divided into actively and passively driven flow system. The fluid flow driving mechanism will be further discussed in Section 2.4.

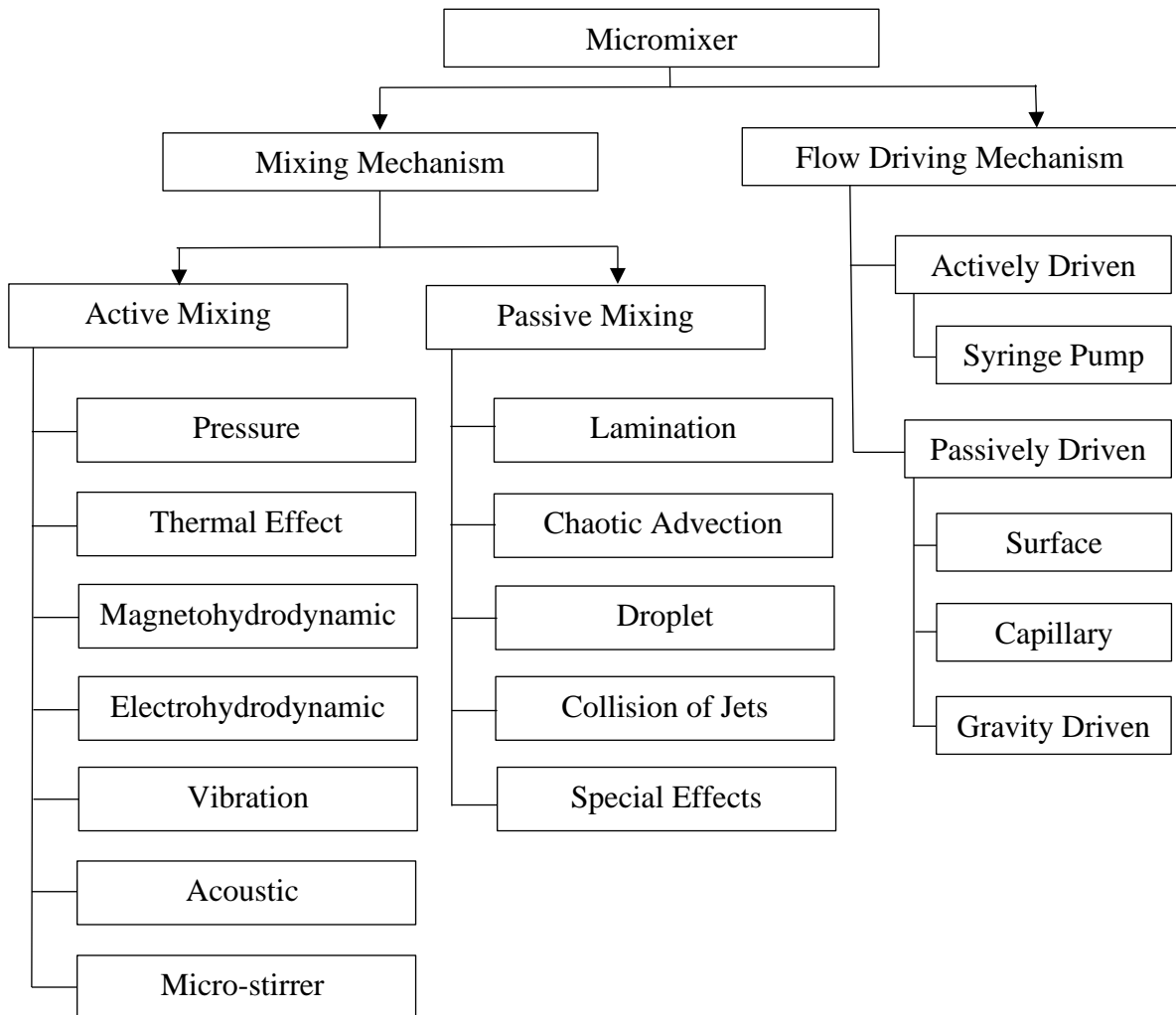


Figure 2.1: An Overview of Mixing and Flow Driving Mechanism of Micromixer

2.3.1 Active Mixing

Active mixing uses provision of external energy to achieve a relatively high mixing efficiency. This is because low Reynolds number typically experienced in the microfluidic system due to small microchannel features and dominant viscous effect compared to inertial forces causes low mixing performance, as shown in Equation 2.1:

$$Re = \frac{\textit{Inertial effects}}{\textit{Viscous effects}} = \frac{\rho v D}{\mu} \quad \text{Equation 2.1}$$

where ρ is density of the fluid, v is velocity of the fluid, D is hydraulic diameter of channel and μ is dynamic viscosity of the fluid. Therefore, external energy through actions of relevant actuators are needed to boost the mixing process by stretching and folding of the fluid mixture (Kumar et al., 2011). Active mixing can be classified into several categories according to their actuator disturbance generation methods such as pressure, thermal effect, magnetohydrodynamic, electrohydrodynamic, vibration, acoustic and micro-stirrer as shown in Figure 2.1.

Chen et al. (2016a) studied the effect of artificial cilia, which based on pressure disturbance mechanism on mixing performance of micromixer. The study involved numerical simulation and experimental analysis using micro-PIV system for four different beating mechanism of artificial cilia. It was shown that beating pattern and followed flow trajectory of the artificial cilia play an important role towards mixing performance of the micromixer. Shamsoddini (2018) investigated temperature ratio (thermal effects) on mixing performance of active micromixer. The proposed method was to reduce the viscosity of the liquid by increasing the temperature which in turn increases molecular diffusion rate. This

simultaneously promotes vortex formation and significantly increases mixing efficiency as a result of reduced viscosity.

Nouri et al. (2017) performed rapid mixing of deionized water and ferrofluid liquid using magnetohydrodynamic concept in Y-shaped microfluidic device. The effects of different magnetic field strength and flow rate towards mixing performance were done by both numerical simulation and experiment. It was found that magnetohydrodynamic mixing significantly increase the mixing efficiency. However, mixing efficiency was found to reduce with the increase of flow rate. Kim et al. (2018) studied the effects of electrodes configuration towards mixing performance of electrohydrodynamic micromixer. Potential difference generated by the electrodes creates nonuniform flow of microparticles inside the system which in turn increases the mixing efficiency. Therefore, it is more effective to generate different potential along the flow path to achieve maximum mixing.

Liu et al. (2018) utilized vibration based on piezoelectric to enhance mixing performance. The experimental results show that the vibration system can be used to generate vortices and active convection mixing, which in turn increase the mixing efficiency. Agglomeration and deposition of the mixing reactant can be reduced by increasing the driving voltage of the system. In a different study, Faryadi et al. (2014) investigated the effect ultrasonic wave towards micromixing performance. They found that the mixing process was enhanced (lower segregating index) with the activated ultrasonic transducer. The effects of different geometry and volume flow rate ratio towards mixing performance with and without ultrasonic irradiation were discussed. It was found that mixing efficiency were reduced when volume flow rate ratio increases for both with and without ultrasonic

irradiation. In addition, difference in mixing performance at lower and higher volume flow rate are more significant when the transducer was turned on.

Jafarian et al. (2014) modelled active micromixer with different rotational arrangement and angular velocity of micro stirrers to study the effect of these parameters towards mixing efficiency. The model was constructed using smoothed particles hydrodynamics method to analyse flow field and diffusion of two miscible fluids. The study shows that rotational arrangement of micro stirrers is a crucial parameter towards mixing performance. Furthermore, mixing efficiency of the system can be increased by decreasing the inlet Reynolds number or increasing angular velocity of the micro stirrer. Of many active mixing mechanisms, stirrer type mixing provides the fastest, most efficient mixing and flexibility for many fluid types (Khozayemeh-Nezhad & Niazmand, 2018). This corroborates well with finding reported by Jafarian et al. (2014); (Park et al., 2008); Ryu et al. (2011); Shamsoddini et al. (2016).

In short, mixing in active micromixer much easier to control externally even though they are difficult to fabricate (Ward & Fan, 2015). The system that utilize active mixing principles have substantially higher mixing performance at the expense of complex and sophisticated design (Cortelezzi et al., 2017). For this reason, passive mixing mechanism is preferable for some applications.

2.3.2 Passive Mixing

Fundamental concept behind passive micromixing is enhancement of diffusive effects between fluids. In order to achieve this, contact surface area between the mixing samples must be increased. Other than that, residence time or contact time between the fluids should be increased. One of the approaches to increase the contact surface and residence

time is by manipulating the microfluidic channels' geometry, pattern and surface (Ward & Fan, 2015). As shown in Figure 2.1, passive mixing can be classified into several categories based on their mixing enhancement mechanism.

In lamination category, the most common mixing mechanism is T- and Y-micromixers (Sarkar et al., 2014) where two streams of fluid are brought together towards a single microchannel. Once the mixing fluids meet in the single microchannel, molecular diffusion starts to occur across the fluids' interfaces. However, due to large Peclet number (Pe) as shown in Equation 2.2, this mixing is typically slow such that a very long microchannel is required (Ward & Fan, 2015) resulting in ineffective mixing in the absence of heat transfer.

$$Pe = \frac{Lv}{D_m} \quad \text{Equation 2.2}$$

where L is characteristic length of the channel and D_m is mass diffusion coefficient. In the context of heat transfer (Rapp, 2016), Pe can be written as shown in Equation 2.3.

$$Pe = \frac{Lv}{\alpha} \quad \text{Equation 2.3}$$

where α is thermal diffusivity coefficient.

Instead of using standard T- and Y-micromixers, parallel lamination was utilized to further increase the mixing efficiency (Capretto et al., 2011). The concept of parallel lamination is that the main sample fluids will be split into several smaller microchannels and at certain point these fluids will be joined together to form laminated fluids with increased interface area. This mixing mechanism was also applied in gradient reactor with network microchannels (Jeon et al., 2000). In addition, hydrodynamic focusing (Jiang et al., 2013;

Lu et al., 2016) can be used to increase mixing efficiency. A smaller and thinner stream of sample fluid will be supplied to main channel where mixing time are proportional to the focused stream width (Capretto et al., 2011). This would lead to a significant increase in mixing as the focused stream width is reduced. Split and recombine micromixer or also known as sequential lamination micromixers (Nimafar et al., 2012) is another commonly used micromixer. This type of micromixer uses sequential process of splitting and recombination for several times to enhance mixing.

Additionally, chaotic advection is another alternative for enhancing mixing. Compared to standard advection which occurs in horizontal direction, chaotic advection generally occurs in multiple directions generating transverse flow which causes rapid growth in contact area between the mixing fluids. Appropriate geometrical manipulation will stretch, fold, break, and split the laminar flow inside the microchannel. The most straightforward method to alter the flow direction and create recirculation inside the flow system is by introducing obstacles inside the microchannel (Chen & Zhao, 2017; Heshmatnezhad et al., 2017). The whirl flow created by this method will produce transversal mass flow which increases mixing efficiency. 3D serpentine (Chen et al., 2016b), zigzag (Ta et al., 2015), sequential logarithmic shape (Scherr et al., 2012) and sinusoidal shaped (Parsa et al., 2014) are some approaches of geometric manipulations that induce chaotic advection through consecutive formation of Dean vortices. Dean vortices which comprise of two tangentially opposite vortices are usually formed when the fluids pass through curved path (Shamloo et al., 2017). This swirling motion are characterized by a dimensionless number, Dean number (De) as shown in Equation 2.4.

$$De = Re \sqrt{\frac{D_h}{2R_c}} \quad \text{Equation 2.4}$$

where D_h is hydraulic diameter of the channel and R_c is the radius of curvature of the curved path.

Furthermore, the abrupt changes in the shape of microchannel will promote faster mixing with transverse velocity components localized at certain channel walls (Capretto et al., 2011). Another effective method to increase mixing performance is by introducing patterns on the walls of the microchannels such as cylindrical grooves (Wang et al., 2012) and herringbone (Chen & Wang, 2015). In one study, a standard T-shaped micromixer with straight microchannel requires twice mixing length as compared to staggered-herringbone micromixer (Capretto et al., 2011).

In addition to geometrical manipulation that involves miscible fluids, mixing performance can be enhanced through formation of droplets in a multiphase flow. Due to immiscibility of the droplet with surrounding fluids, the mixing reagent will remain concentrated and localized inside their respective droplets (Ward & Fan, 2015). Sakurai et al. (2018) utilized immiscibility droplet injection frequency to generate disorder on the mixing interface. This method enables controlled mixing since the mixing efficiency increases with the increase of droplet injection frequency. Collision of jets had been applied in a chemical reactor to achieve a high mixing efficiency. Gao et al. (2015) studied the effect of collision velocity, nozzle diameter and acid concentration to obtain minimum micromixing time. It was found that this method provides a better mixing efficiency compared to conventional stirred tank. Xu & Chu (2015) utilized Coanda effect to enhance mixing in oscillating feedback micromixer. The study involved several designs having

feedback and splitter configurations. It was reported that by utilizing Coanda effect, asymmetric oscillating feedback micromixer with a splitter provide the highest mixing performance among the three designs.

Table 2.1 provides a summary for this section that includes the discussed types of mixing and their categories.

Table 2.1: Summary of Mixing Mechanisms

Type of Mixing	Method		Description/examples	Reference
Active Mixing	Pressure		Influence of artificial cilia actuation in microchannel towards micromixing	Chen et al. (2016a)
	Thermal effects		Thermal effect on mixing rate in active micromixer with rotating stirrer	Shamsoddini (2018)
	Magnetohydrodynamic		Rapid mixing of deionized water and Fe ₃ O ₄ ferrofluid assisted by magnetic field	Nouri et al. (2017)
	Electrohydrodynamic		Influence of AC voltage induced coplanar meandering electrode towards mixing	Sasaki et al. (2006)
	Vibration		Self-circulation micromixer integrated with vibrational system based on piezoelectric drive technology	Liu et al. (2018)
	Ultrasound		Study on the effects of ultrasound towards mixing performance	Faryadi et al. (2014)
	Micro-Stirrer		Effects of disturbance induced by oscillating micro-stirrer towards mixing	Park et al. (2008)
Passive Mixing	Lamination	Junction manipulation	Evaluation of mixing for different 1-1 and 1-2 microfluidic junctions	Sarkar et al. (2014)
		Multiple parallel lamination	Gradient mixing inside network microchannel	Jeon et al. (2000)
		Hydrodynamic focusing	Formation of aromatic organic nanoparticle by hydrodynamic focusing mixing	Jiang et al. (2013)
		Series	Mixing enhancement of using H-shaped split and recombination microchannel	Nimafar et al. (2012)

Table 2.1 continued

	Chaotic advection	Obstacles	Layout design optimization employing obstacles in three-dimensional passive micromixer	Chen & Zhao (2017)
		Patterned wall	Mixing enhancement using fabricated cylindrical grooves in straight microchannel	Wang et al. (2012)
		3D serpentine	Study of mixing performance in serpentine micromixer by experiment and numerical simulation	Chen et al. (2016b)
		Zigzag	Effects of geometric parameters for trapezoidal-zigzag micromixer towards mixing performance	Ta et al. (2015)
	Droplet		Thrust of droplets into mixing interface in passive micromixer	Sakurai et al. (2018)
	Collision of jets		Effects of different impinging velocity in impinging jet reactor towards micromixing	Gao et al. (2015)
	Special effects		Micromixers design utilizing Coanda effects characterized by different feedback and splitter configuration	Xu & Chu (2015)

2.3.3 Passive Micromixer Designs

This section reviews some designs of passive micromixers based on geometrical modification.

2.3.3.1 T- and Y-shaped Micromixers

Sarkar et al. (2014) evaluated mixing efficiency of different microfluidic junctions, namely 1-1 and 1-2 junctions. The junction types were characterized by concept of skewness at the inlet junction, or in other words, the average value of the angles between inlet channels and main channel. Validation of preliminary numerical simulation was conducted by comparing Y-micromixer simulation results with experimental data and theoretical results. The experiment was conducted with a similar preliminary simulation model with 750 μm microchannel diameter. One of the inlets was applied with colourless water and the other

inlet was applied with dyed water. Image acquisition and analysis of the device was performed using high speed camera on different flow rate conditions for both inlets (Sarkar et al., 2014). This study shows that asymmetric junctions give a better mixing performance for both type of mixing junctions. Furthermore, mixing performance in 1-2 microfluidic junctions was found better as compared to 1-1 microfluidic junction.

2.3.3.2 Split and Recombination

Ansari et al. (2010) designed a passive O-shaped micromixer incorporating unbalanced splits and recombination mixing mechanism (refer Figure 2.2). The main channel width was $300\ \mu\text{m}$ which equals to the width of two sub-channels. The difference in microchannel width was the primary cause of the unbalanced collisions due to unequal fluid flow in both microchannels. Analysis of mixing efficiency for different width ratio, W_1/W_2 of 1.0, 1.4, 1.72 and 2.0 at different Reynolds number shows that unbalanced collisions cause significant distortion. It was also found that higher mixing efficiency was attainable at $W_1/W_2 = 2$. The maximum mixing efficiency except at $Re = 10$ shows that unbalanced collision was not very effective at low Reynolds number because of low inertial forces formed. On the other hand, rapid mixing was observed at $Re > 40$.

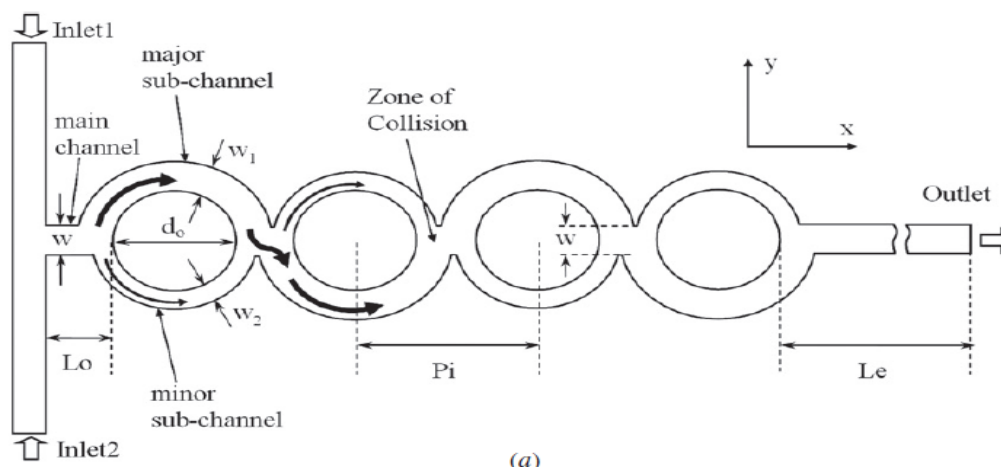


Figure 2.2: Geometrical Configuration of Unbalanced Splits and Collisions Microfluidic Device (Ansari et al., 2010)

Nimafar et al. (2012) compared H-shaped micromixer with the T-shaped and O-shaped micromixers. The width, height and total length of the microchannels are $400\ \mu\text{m}$, $400\ \mu\text{m}$ and $21\ \text{mm}$, respectively. The change in the dye colour intensity was used to determine the mixing efficiency calculated using grayscale images. The experiment was conducted at very low Reynolds number, $0.08 < \text{Re} < 4.16$. Results of the experiment showed that mixing index at the end region after $20\ \text{mm}$ ($\text{Re} = 0.083$) for T-micromixer, O-micromixer and H-micromixer are 38% , 55% and 92% , respectively.

Le The et al. (2015) proposed microfluidic device based on shifted trapezoidal blades (STB) design with the aim to achieve complete mixing within a short period of time. The STB design essentially incorporated several mixing mechanisms namely, unequal splitting and recombining, converging and diverging, recirculation, and twisting (Le The et al., 2015). A significantly improved mixing was obtained attributed to asymmetrical splitting and recombining nature which eventually lead to chaotic advection. It was found that mixing of these fluids is highly dependent on diffusion effect for low regime $\text{Re} \leq 1$. In the regime of $1 \leq \text{Re} \leq 5$, the flow rate is not high enough to produce vortices. At the same time, the molecular diffusion was reduced causing the mixing efficiency decrease with increasing of Reynolds number. When flow reached $5 \leq \text{Re} \leq 40$, the mixing efficiency increases due to presence of chaotic advection. In the regime of $\text{Re} \geq 40$, the efficiency slightly decreased with increasing of Reynolds number because of short residence time and reduced molecular diffusion. The highest mixing efficiency which is around 95% was obtained at $\text{Re} = 40$.

Sivashankar et al. (2016) laser-fabricated a 3D twisted passive micromixer that utilizes both splitting and recombining and chaotic advection as means of mixing enhancement mechanism. It was observed that the surface roughness due to fabrication

method by laser can induce vortices and eddies. The result interestingly shows that the three mixing units were enough to achieve full mixing where after three mixing units the concentration of the flow is almost constant.

Chen et al. (2018) compared two multi-layer micromixers: F-micromixer and E-micromixer. From $Re = 0.5$ to $Re = 15$, mixing efficiency was found to be decreasing with increasing of Reynolds number since mixing depend on molecular diffusion only. The mixing efficiency was found to be the lowest at $Re = 15$. When $Re > 15$, mixing efficiency were increased with increasing of Reynolds number since convection effects start to become dominant (Chen et al., 2018). Once the $Re > 25$, all these micromixers' mixing efficiency were significantly increased. Mixing efficiency of F-micromixer and E-micromixer for $Re = 80$ were 92 % and 94 %, respectively.

Shah et al. (2019) evaluated mixing index due to chaotic advection of standard Y-micromixer, Y-shaped circle split and recombination (YCSAR), Y-shaped rhombus-circle split and recombination (YRCSAR) and Y-shaped rhombus split and recombination (YRSAR) (refer Figure 2.3). These micromixers were designed with same dimension such that their channel width, channel depth and total length are $300 \mu\text{m}$, $200 \mu\text{m}$ and 30 mm , respectively. YCSAR, YRCSAR and YRSAR were used to induce chaotic advection mixing through formation of Dean effect and transverse flow that eventually amplify the mixing effect (Shah et al., 2019). YRCSAR demonstrated the highest mixing efficiency followed by YCSAR, YRSAR and standard Y-micromixer.

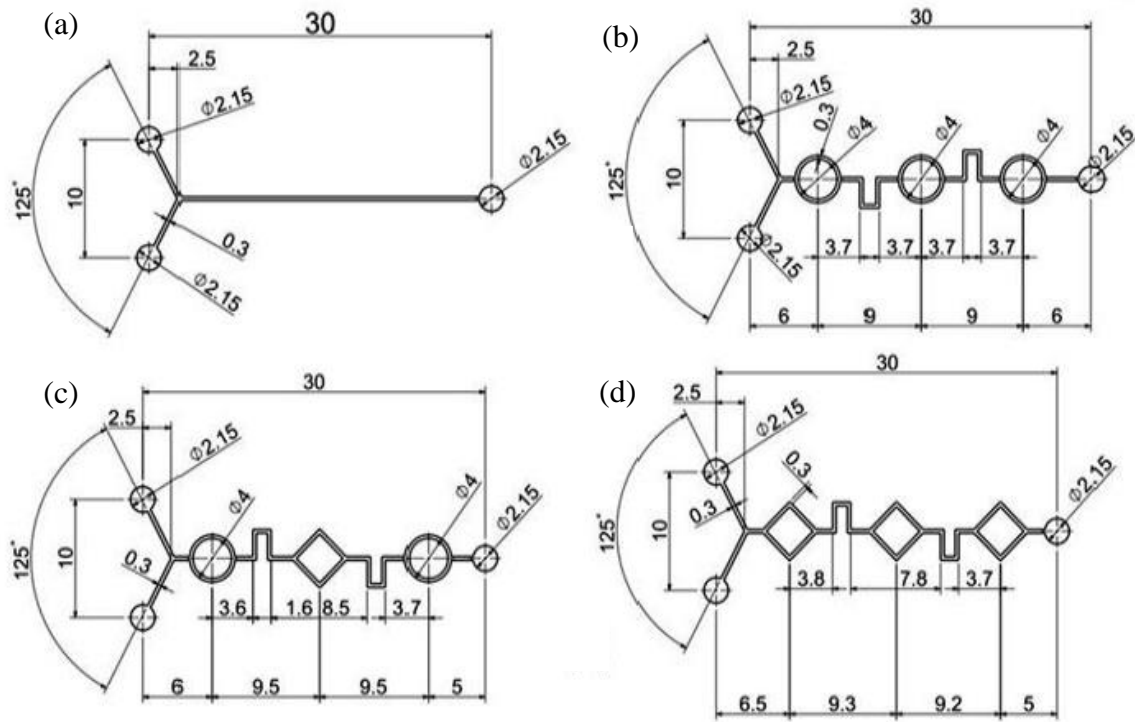


Figure 2.3: Different Geometrical Configuration Used in This Study (Units in mm)
 (a) Standard Y-Micromixer With Straight Mixing Channel (b) YCSAR
 (c) YRCSAR (d) YRSAR (Shah et al., 2019)

2.3.3.3 Shape of Microchannels

Scherr et al. (2012) performed numerical simulation and experiment on mixing index of a micromixer designed based on logarithmic spirals (refer Figure 2.4). Mixing index and pressure drop at different Reynolds numbers were compared with scaled models of Archimedes (Sudarsan & Ugaz, 2006), Meandering-S (Jiang et al., 2004) and standard T-channel. Formation of Dean vortices at the curved channels was found enhances the mixing process. Moreover, the mixing efficiency was found increases once $Re > 15$ because of transition between diffusive mixing to convective mixing (Scherr et al., 2012). The results showed that mixing efficiency in logarithmic spirals are 10 % - 15 % higher compared to Archimedes and Meandering-S micromixers.

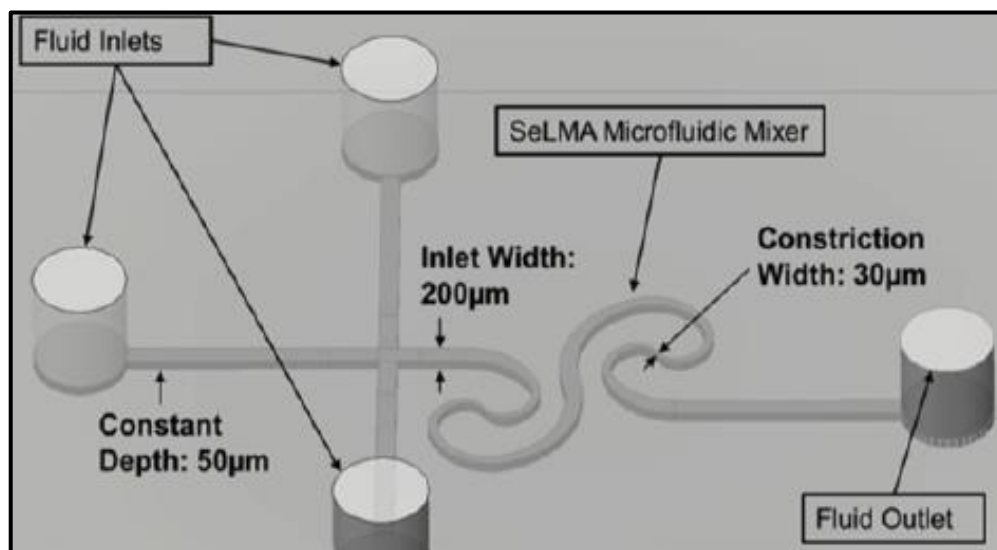


Figure 2.4: Configuration of SeLMA Micromixer (Scherr et al., 2012)

Li et al. (2012) performed a study on mixing efficiency for zigzag micromixer. A standard Y-junction mixer with identical mixing length and channel dimension was designed to perform mixing performance comparison with the developed zigzag micromixer (turning angle 35° and $20 \mu\text{m}$ outlet channel). It was found that the mixing in zigzag micromixer is significantly better compared to the standard Y-junction mixer.

Parsa et al. (2014) performed both experiment and numerical simulation to study relationship between ratio of amplitude to wavelength of convergent-divergent sinusoidal shaped micromixer (Refer Figure 2.5). The sinusoidal shaped micromixers were varied by their ratio of amplitude to wavelength and their aspect ratio of microchannel cross section. It was reported that the mixing indices increase in shorter mixing length as the ratio of amplitude to wavelength increases. Furthermore, it was also found that the mixing index improved while pressure drop reduced with the increasing aspect ratio of microchannel cross section.

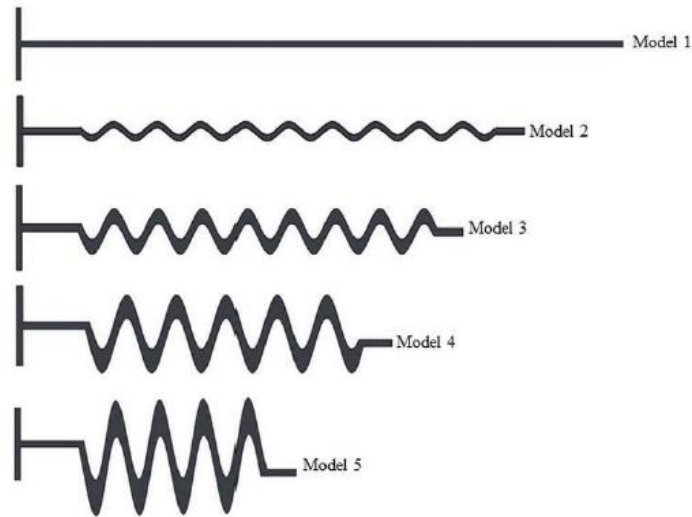


Figure 2.5: Top View of Different Designs of Microfluidic Devices (Parsa et al., 2014)

A study on mixing performance of micromixer with serpentine microchannel was carried out by Chen et al. (2016b). Results of six different geometries indicate that the mixing efficiency decreases with the increase of Re from 0 to 0.1, predominantly governed by molecular diffusion. Furthermore, mixing efficiency is determined by residence time at low Reynolds number. When Re increases from 1 to 100, mixing performance increases due to convection. In addition, result showed a higher mixing efficiency and higher-pressure drop in square-wave micromixer compared to multi-wave micromixer and zigzag micromixer (Chen et al., 2016b).

2.3.3.4 Patterned walls

The effect of additional grooves in passive micromixer using three different geometrical configurations was studied by Wang et al. (2012). The objective of the grooves with different dimensions (100, 200 and 300 μm grooves depth) were to ensure convection flows occurs once the laminar flow passing through the grooves, which in turn will enhance the mixing process. Experimental and simulation results proved that the mixing performance

increases significantly using these designs for $1.0 < Re < 100$. The groove depth of $100 \mu\text{m}$ shows the highest mixing efficiency.

Kwak et al. (2016) studied the effects of positive staggered herringbone mixer (SHM) towards mixing performance. Mixing efficiency of this positive SHM was compared with negative SHM. SHM with forward flow direction had higher mixing efficiency compared to that of reverse flow direction. Positive SHM with both forward and reverse flow direction mixed the fluids completely after two cycles while negative SHM with forward and reverse flow direction mixed the fluids completely after four and five cycles, respectively. Table 2.2 summarizes enhancement methods of the discussed passive micromixers.

Table 2.2: Summary of Key Findings for Mixing Enhancement in Passive Micromixers

Passive micromixer design	Material	Analysis Method	Finding/Remark
T- and Y-shape with various angles (Sarkar et al., 2014)	Not specified	<ul style="list-style-type: none"> Numerical Simulation Experiment-dye visualization test 	<ul style="list-style-type: none"> Asymmetric junctions give a better mixing performance 1-2 microfluidic junction is found to be better compared to 1-1 microfluidic junction
Unbalanced split and recombination of O-micromixer (Ansari et al., 2010)	PDMS by photolithography	<ul style="list-style-type: none"> Numerical simulation Experiment – fluorescent visualization test 	<ul style="list-style-type: none"> Unbalanced collisions between mixing fluids cause significant distortion Re = 10 shows that unbalanced collision is not very effective due to low inertial forces $10 \leq Re \leq 80$
Split and recombination of H-micromixer (Nimafar et al., 2012)	PMMA by CNC engraving and milling	<ul style="list-style-type: none"> Experiment-blue and yellow dye visualization test 	<ul style="list-style-type: none"> Re = 0.083, mixing efficiency at region after 20 mm for T-micromixer, O-micromixer and H-micromixer are 38 %, 55 % and 92 %, respectively. $0.08 < Re < 4.16$

Table 2.2 continued

<p>Split and recombination of shifted trapezoidal blades mixer (Le The et al., 2015)</p>	<p>PDMS by photolithography</p>	<ul style="list-style-type: none"> Numerical simulation Experiment-pH test using phenolphthalein 	<ul style="list-style-type: none"> Unequal cross-sectional area causes variation in fluid velocity which causes unequal collision More efficient mixing due to asymmetrical splitting and recombining $1 \leq Re \leq 5$, mixing efficiency significantly decreased when Re increase. The highest mixing efficiency of 95 % was obtained at $Re = 40$. $0.5 \leq Re \leq 100$
<p>Split and recombination of 3D twisted passive micromixer (Sivashankar et al., 2016)</p>	<p>PMMA by CO₂ laser machining</p>	<ul style="list-style-type: none"> Numerical simulation Experiment-dye visualization test and pH test using phenolphthalein 	<ul style="list-style-type: none"> Mixing efficiency improved due to presence of chaotic advection and vortices at arc shape channel Surface roughness from fabrication improve mixing Three mixing units were enough to achieve full mixing $1 \mu\text{L}/\text{min} \leq \text{Flow rates} \leq 1000 \mu\text{L}/\text{min}$
<p>Split and recombination of F- and E-micromixer (Chen et al., 2018)</p>	<p>PMMA by CNC engraving and milling</p>	<ul style="list-style-type: none"> Experiment-pH test using phenolphthalein 	<ul style="list-style-type: none"> $0.5 \leq Re \leq 25$, presence of molecular diffusion only, mixing efficiency decrease with increasing of Reynolds number $Re > 15$, mixing efficiency were increased with increasing of Reynolds number due to convection effects $Re = 80$, mixing efficiency of SESM and FESM close to 100 % $Re = 0.5, 1, 5, 15, 25, 40, 50, 80$ and 100
<p>Patterned wall (grooves on the microchannel) (Wang et al., 2012)</p>	<p>PDMS by photolithography</p>	<ul style="list-style-type: none"> Numerical simulation Experiment - pH test using phenolphthalein 	<ul style="list-style-type: none"> Design with $100 \mu\text{m}$ cylindrical grooves depth has highest mixing efficiency compared to $200 \mu\text{m}$ and $300 \mu\text{m}$ $Re = 0.1, 1.0, 10$ and 100
<p>Split and recombination of YCSAR, YRCSAR and YRSAR (Shah et al., 2019)</p>	<p>Borosilicate glass and silicone elastomer by 3D printing system</p>	<ul style="list-style-type: none"> Numerical simulation Experiment – mixing between red and blue ink fluid 	<ul style="list-style-type: none"> Mixing efficiency increased due to chaotic advection YRCSAR demonstrated the highest mixing efficiency followed by YCSAR and YRSAR $0.5 \leq Re \leq 100$

Table 2.2 continued

<p>Micromixer based on logarithmic spirals, SeLMA (Scherr et al., 2012)</p>	<p>PDMS by photolithography</p>	<ul style="list-style-type: none"> Numerical simulation Experiment – fluorescent visualization test 	<ul style="list-style-type: none"> Mixing efficiency increase with Re once $Re > 15$ due to transition between diffusive mixing to convective mixing Mixing efficiency of SeLMA are 10 % to 15 % higher compared to Archimedes and Meandering-S design. Dean vortices at the curved channels enhance the mixing process
<p>Zigzag micromixer (Li et al., 2012)</p>	<p>PDMS by soft lithography</p>	<ul style="list-style-type: none"> Numerical simulation Experiment – mixing of sulforhodamine B and fluorescein 	<ul style="list-style-type: none"> Mixing of the developed zigzag micromixer was improved significantly compared to the standard Y-junction Smaller turning angles and smaller outlet channel width will provide better mixing Experimental flow rate = 0.67, 1.67, 5 and 10 $\mu\text{L/s}$
<p>Convergent-divergent sinusoidal shaped micromixer (Parsa et al., 2014)</p>	<p>PMMA by CO₂ laser machining</p>	<ul style="list-style-type: none"> Numerical simulation Experiment – mixing of methylene blue solution and pure water 	<ul style="list-style-type: none"> Mixing index improved and pressure drop reduced with the increasing aspect ratio of microchannel cross section. Ratio of amplitude to wavelength increases, the mixing index increases Slight differences in results because simulation focus on horizontal mid plane while experiment cover the whole depth of microchannel
<p>Serpentine micromixer (Chen et al., 2016b)</p>	<p>PMMA by CNC engraving and milling</p>	<ul style="list-style-type: none"> Numerical simulation Experiment - blue and yellow dye visualization test 	<ul style="list-style-type: none"> Mixing efficiency are decreasing when Re increase from 0 to 0.1 Mixing efficiency are increasing when Re increase from 1 to 100 Higher mixing efficiency and higher-pressure drop-in square-wave micromixer compared to multi-wave micromixer and zigzag micromixer. Re = 0.1, 1, 10 and 100
<p>Patterned wall (Kwak et al., 2016)</p>	<p>PDMS by photolithography</p>	<ul style="list-style-type: none"> Numerical simulation Experiment – fluorescent visualization test 	<ul style="list-style-type: none"> Positive staggered herringbone mixer (SHM) have better mixing than negative SHM Forward flow direction provides better mixing than reverse flow direction

2.4 Passive Flow Driving Mechanism

Increasing demand for microfluidic devices has led to development of active and passive flow driving mechanisms. An active flow driving mechanism usually requires expensive equipment (syringe pump) and power/energy. On the other hand, passive driving mechanism mostly depend on the effects of surface tension, capillary action and gravity, to name a few. The following section discusses some of the passively driven flow mechanism.

2.4.1 Surface Tension

Walker & Beebe (2002) proposed a simple passive fluid driving system that theoretically depends on surface energy to pump liquid from inlet to outlet. This passive technique is governed by Young-Laplace equation (refer Equation 2.5) where smaller drops of liquid possesses higher internal pressure compared to larger drops.

$$\Delta P = \frac{2\gamma}{R} \quad \text{Equation 2.5}$$

where ΔP is pressure difference across fluid interface, γ is surface tension and R is radius of liquid drop. Therefore, the different in pressure gradient will force the water from pumping port (inlet) to reservoir port (outlet). In this case, 100 μL drop of liquid was placed on the reservoir port while 0.5 – 5 μL on pumping port. PDMS was used as the main material to fabricate the microfluidic device due to its hydrophobicity which kept the liquid droplet from spreading out. If somehow the liquid spread out, the Young-Laplace pressure will be reduced and inhibit the system to drive the fluid flow. Additionally, the same pumping method was used to drive the fluid from position with low to higher gravitational potential energy.

2.4.2 Capillary Effects

Mukhopadhyay (2017) studied the effect of surface-area-to-volume ratio in surface-driven capillary flow. Effectiveness of several proposed designs were measured by the time required by the different fluids to travel from inlet port to outlet reservoir. The microfluidic devices were fabricated using PMMA by mask-less lithography in cleanroom, with varying dimension and number of micropillars to achieve different surface-area-to-volume ratio. There is basically one design without any pillars and other 3 designs of 150 μm , 250 μm and 350 μm side length with 342, 214 and 132 individual pillars, respectively. It was demonstrated that the microchannel with larger surface area will increase the time required by the fluid meniscus to travel from inlet port to outlet port (Mukhopadhyay, 2017). Furthermore, ethylene glycol flow based on surface-driven capillary flow inside the microchannel is slower due to its higher viscosity.

2.4.3 Gravity Driven

Analytical model to estimate generated flow rate gravity-driven pumping system was proposed by Mäki et al. (2015), focusing on utilization of hydrostatic pressure generated by gravitational potential energy to move liquid. At the same time, the fluid flow will be reduced as the height difference decreases, lowering the hydrostatic pressure. Considering capillary forces inside the channel are opposite to the movement of fluid by hydrostatic pressure, the flow $Q(t)$ can be calculated using Equation 2.6 (inlet and outlet reservoir have same cross-sectional area).

$$Q(t) = \frac{\Delta p(t)}{R_{hyd}} = \frac{p_{hyd}(t) - \Delta p_{cap}}{R_{hyd}} \quad \text{Equation 2.6}$$

where $\Delta p(t)$ is the total pressure drop, $p_{hyd}(t)$ hydrostatic pressure of incompressible fluid, Δp_{cap} is capillary pressure drop and R_{hyd} hydraulic resistance of the channel. In order to verify this mathematical model, PDMS based microfluidic device was fabricated using standard photolithography process with different vertical channel widths of 50, 100, 250 and 500 μm . Comparison between the model and experimental result shows that the proposed model can estimate the height difference at improved accuracy due to the fact that it considers capillary pressure drop in the equation (Mäki et al., 2015). Model that does not consider the capillary pressure drop will overestimate the effectiveness of pumping and will reduce the accuracy of results.

2.5 Characterization of Mixing Performance

Mixing performance micromixers are generally characterized as a function of mixing index. On the basis of colour changes, the mixing index has been employed to characterize mixing between dye coloured liquids (Chen et al., 2016b; Sarkar et al., 2014; Shah et al., 2019), reaction between chemical that produces different coloured species (Li et al., 2012), reaction between pH indicators (Chen et al., 2018; Le The et al., 2015; Sivashankar et al., 2016) and dilution of fluorescent liquids (Ansari et al., 2010).

Several quantitative mixing indices have been defined based on intensity images recorded using typical digital video microscopes (Ansari et al., 2010; Le The et al., 2015; Nimafar et al., 2012; Wang et al., 2018). The digitally captured intensity images are usually stored in the format of three 8-bit monochromatic red, green and blue colours, which can be converted to the grayscale, Cyan/Magenta/Yellow/Key (CMYK) or Hue/Saturation/Intensity (HSI) colour model. The mixing index can be calculated using

grayscale images as shown in Equation 2.7 (Chen et al., 2016b; Le The et al., 2015; Nimafar et al., 2012; Wang et al., 2018):

$$Mixing\ index = 1 - \sqrt{\frac{1}{N} \sum_{i=1}^N \left(\frac{\bar{I}_{gray,i} - I^*}{I^*} \right)^2} \quad \text{Equation 2.7}$$

where N is the total number of pixels i analysed, I^* is the expected normalized pixel intensity which equals to 0.5 (Nimafar et al., 2012), and $\bar{I}_{gray,i}$ (Jännig & Nguyen, 2011) is

$$\bar{I}_{gray,i} = \frac{(I_{gray,i} - I_{gray,min})}{(I_{gray,max} - I_{gray,min})} \quad \text{Equation 2.8}$$

where $\bar{I}_{gray,i}$ is the normalized pixel intensity inside the image while $I_{gray,min}$ and $I_{gray,max}$ are the minimum and maximum local pixel intensity, respectively, and $I_{gray,i}$ (ITU, 2011) is

$$I_{gray,i} = (0.299R + 0.587G + 0.114B)/3 \quad \text{Equation 2.9}$$

where $I_{gray,i}$ is the local pixel intensity.

The main limitation of Equation 2.7 is that the expected normalized pixel intensity, I^* is treated as a constant. In practice, the actual constant value of I^* does not necessarily equal 0.5 depending instead on the measured pixel intensity of a premixed solution. To incorporate this into the calculation of mixing index, the following Equation 2.10 has been proposed for HSI images (Chen & Wang, 2015; Fu et al., 2017; Johnson et al., 2002; Sivashankar et al., 2016):

$$Mixing\ index = 1 - \sqrt{\frac{1}{N} \sum_{i=1}^N \left(\frac{(\bar{I}_{HSI,i} - \bar{I}_{HSI,mix})}{(\bar{I}_{HSI,unmix} - \bar{I}_{HSI,mix})} \right)^2} \quad \text{Equation 2.10}$$

where $\bar{I}_{HSI,mix}$ is the normalized premixed pixel intensity, $\bar{I}_{HSI,unmix}$ is the normalized pixel intensity prior to mixing, and $\bar{I}_{HSI,i}$ (Fu et al., 2017) is

$$\bar{I}_{HSI,i} = \frac{(I_{HSI,i} - I_{HSI,min})}{(I_{HSI,max} - I_{HSI,min})} \quad \text{Equation 2.11}$$

where $\bar{I}_{HSI,i}$ is the normalized pixel intensity inside the image while $I_{HSI,min}$ and $I_{HSI,max}$ are the minimum and maximum local pixel intensity, respectively, and $I_{HSI,i}$ (Fu et al., 2017) is

$$I_{HSI,i} = (R + G + B)/3 \quad \text{Equation 2.12}$$

It is noted that Equation 2.10 is valid for both HSI and grayscale images. In time-series micromixing experiments (McDonough et al., 2019; Surdo et al., 2017; Yamamoto et al., 2013; Zha et al., 2018), $\bar{I}_{HSI,mix}$ can no longer be considered constant. This is because the value of $\bar{I}_{HSI,mix}$ varies with respect to a particular image frame. In other words, $\bar{I}_{HSI,mix}$ is frame-dependent. To accommodate frame-varying mean intensity into the calculation of mixing index, the following Equation 2.13 has been proposed (Engler et al., 2004; Fu et al., 2017; Luo et al., 2006; Parsa et al., 2014; Rafeie et al., 2017; Shah et al., 2019):

$$Mixing\ index = 1 - \sqrt{\frac{\frac{1}{N} \sum_{i=1}^N (\bar{I}_{HSI,i} - \bar{I}_{HSI,avg})^2}{\bar{I}_{HSI,avg} (1 - \bar{I}_{HSI,avg})}} \quad \text{Equation 2.13}$$

where $\bar{I}_{HSI,avg}$ is the average value of the entire pixels contained in a single image frame.

The three abovementioned equations (Equation 2.7, Equation 2.10 and Equation 2.13) are essentially based on dispersion (homogeneity) information of the intensity images. One common and clear limitation is that the individual RGB values are first averaged (Equation 2.9 and Equation 2.12) before mixing index is computed.

2.6 Fabrication Method

Microfluidics fabrication primarily depends on the intended application, cost and chemical/mechanical characteristics of the base substrate. This section discusses common methods used to fabricate microfluidic devices, as shown in Figure 2.6.

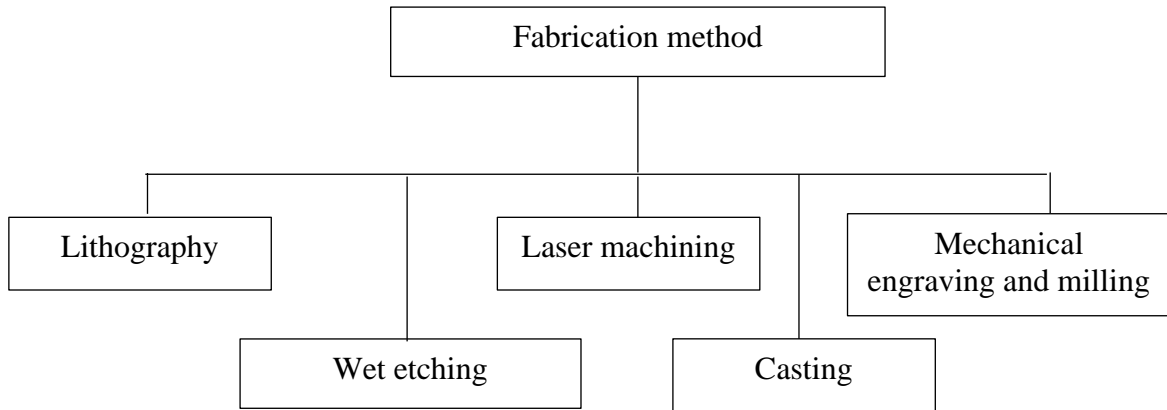


Figure 2.6: Fabrication Methods of Microfluidic Devices

2.6.1 Lithography

PDMS is widely used materials in microfluidics system due to its desirable characteristics such as high gas permeability, optical transparency and biocompatibility (Hou et al., 2017). Besides, various microchannel structures can be fabricated and replicated through a few simple steps such as mixing, casting and heating. Scherr et al. (2012) studied mixing performance of logarithmic spiral with Archimedes and Meandering-S micromixer designs, fabricated by soft lithography fabrication method using master moulds SU-8 2025.

The SU-8 was spun on silicon wafer to achieve thickness of 50 μm . Sylgard 184 (Dow Corning, Midland, MI) and curing agent with ratio of 10:1 was used to fabricate the final device.

Wang et al. (2012) chose PDMS to study the effect of additional cylindrical grooves along microchannel wall on mixing performance. Masters for these microfluidic devices were fabricated using standard lithography process where 100 μm SU-8 layer was spun onto a wafer before exposing to UV light (365 nm). The height of SU-8 are $98 \pm 4 \mu\text{m}$. Liquid PDMS was poured onto the master together with silicone elastomer base and curing agent (Sylgard 184, Dow Corning, USA) with ratio of 10:1. The PDMS mixture was cured at 80 °C for 4 hours until a solid transparent PDMS was formed. The inlet and outlet holes of the microfluidic devices were created by punching them with a blunt needle. The PDMS that was peeled from the master was bonded together with glass slide by means of plasma treatment.

2.6.2 Laser Micromachining

PMMA is one of the key materials for microfluidic devices. Rather than using silicone, glass or quartz which technically involve a series of complex manufacturing processes, PMMA is preferred due to its optical transparency and cost effectiveness (Prakash & Kumar, 2015). In addition, PMMA possesses other technical advantages such as resistance to hydrolysis and chemical inertness in neutral aqueous solutions (Hong et al., 2010). Laser micromachining often used in fabrication of PMMA based microfluidic device (Joanni et al., 2015; Prakash & Kumar, 2015). It involves absorption of laser photon which leads to temperature increase and evaporation of the materials.

Chen et al. (2016c) fabricated a microfluidic device entirely from PMMA using CO₂ laser micromachining. The design of the device was based on four layers of chip instead of two layers of conventional chip. It was reported that the degree of sensitivity for laser cutting parameters on PMMA can be ranked accordingly from cutting speed, laser power, number of passes and channel length (from highest to lowest) at 5 mm/s, 5.4 W, 1 pass and 40 mm, respectively. Width error of the channel of $\pm 5 \mu\text{m}$ and mean roughness of 170 nm were reported for these parameters. One-time bonding technology with a range of temperatures between 70 °C to 103 °C and pressures between 0 MPA to 1.2 MPA was studied to bond all four layers of PMMA chip together.

Prakash & Kumar (2015) conducted a study on the effect of CO₂ micromachining process on fabrication of PMMA based microchannels. A CO₂ laser having maximum power, wavelength and beam focus diameter of 60 W, 10.6 μm and 237 μm , respectively, was used in this study. It was found that maximum width occurs at the highest power combined with lowest speed and lower pulse per inch. The softened zone can be minimized by reducing laser power and increasing the laser speed. Other than that, the most effective depth can be obtained at 700 pulse per inch with 71 % overlapping.

Hong et al. (2010) fabricated microfluidic devices using CO₂ laser through direct writing-ablation of PMMA. The fabrication process utilized CO₂ laser with maximum power, wavelength and scanning speed of 12 W, 10.6 μm and 5 to 500 mm/s, respectively. The ablation process was performed using two setups namely focused laser beam and unfocused laser beam. The laser power and scanning speed were set within ranges of 1.2 to 4.0 W and 50 to 150 mm/s, respectively. Glass cover plates were drilled with inlet and outlet holes prior to thermal bonding process in hot embossing machine for 20 min at 105 °C and

pressure of 5 kg/cm^2 . It was found that focusing method produced microchannel with surface roughness exceeding $1 \mu\text{m}$ which is not suitable for microfluidic application. In comparison, optimized parameters for unfocused method with unfocused length of 40 mm, laser power of 2.4 W and scanning speed of 80 mm/s yielded lowest surface roughness.

Yap et al. (2013) utilized 1.5 mm thick stainless-steel pinholes integrated into commercial CO_2 with maximum output of 40 W and wavelength of $10.6 \mu\text{m}$ to fabricate microchannel. By integrating $50 \mu\text{m}$ (laser power of 16 W) and $35 \mu\text{m}$ (laser power of 28 W) diameter pinholes, the ablated microchannel width can be reduced to 54.2 and $36.4 \mu\text{m}$, respectively using maximum speed of 20 mm/s. Furthermore, the bulges found around the ablated microchannel can be reduced to less than $0.8 \mu\text{m}$ using the pinholes. After ablation, inlet and outlet holes were drilled using 3 mm drill bit, followed by lamination bonding of these two substrates using an office laminator at temperature of $150 \text{ }^\circ\text{C}$.

2.6.3 Mechanical Engraving and Milling

Chen et al. (2016b) studied mixing performance of PMMA micromixer with serpentine microchannel and compared it with other typical geometries. Fabrication process was performed using CNC engraving and milling machine. Milling process parameter with 0.2 mm cutting diameter, 1500 per minute cutting speed and 10,000 rpm were used. Once completed, ultrasonic cleaner was used for cleaning. Following that, hot embossing and bonding machine were employed to complete the fabrication process.

Ogilvie et al. (2010) developed PMMA-based microfluidic devices using automated micro-milling machine. They used PMMA sheets with thickness ranging from 1.5 mm to 8 mm and olefin copolymer wafer with thickness of 0.7 mm and 1.2 mm. Solvent vapour treatment was used to improve surface quality and at the same time irreversibly bond the

chips together. After microchannels fabrication, the substrates were rinsed with isopropyl followed by ethanol and dried with nitrogen. The substrates were placed around 2 mm above 30 ml of solvent at temperature of 25 °C for 4 minutes. The substrates were then transferred for hot press at preheated temperature of 65 °C and pressure of 140 N cm⁻² for 20 minutes. The substrates were then actively cooled down at room temperature over 10 minutes before removing from the press to allow it to settle for 12 hours. Typical surface roughness measured on the microchannels without solvent vapour treatment were measured to be around 100 to 200 nm using atomic force microscope. Using solvent vapour treatment, the surface roughness was reduced to less than 15 nm which is considerably close to virgin substrate's roughness of less than 5 nm.

2.6.4 Casting

Epoxy resin is another type of polymer that possess characteristics suitable for microfluidic applications. It has high Young's modulus, solvent resistant and high optical transparency. Young's modulus for the epoxy can be manipulated by adjusting mixing ratio of resin and hardener. Cheng et al. (2017) fabricated epoxy based microfluidic devices with mixing ratio of 2.5:1 (resin to hardener). The compatibility of this epoxy based microfluidic devices have been demonstrated on three typical microfluidic applications, namely on-chip polymerase chain reaction (PCR) amplifications, multilayer PDMS microvalves and high-speed flow cytometry. Cheng et al. (2017) demonstrated great biocompatibility of the epoxy as it shows no inhibition to cell growth, proving that a commercially available epoxy resin can be used for rapid fabrication which can even surpass PDMS. This is because epoxy does not deform at high flow rate application, for example high flow speed flow cytometer (Goda et al., 2012).

2.6.5 Wet Etching

Glass based microfluidic devices possess advantages over other conventional material such as PDMS due to its non-deformable characteristics. Furthermore, glass is found to be chemically resistant, easy to clean and has rigid structure. Therefore, it is suitable for applications that require high optical transparency and low fluorescence background. Witkowski et al. (2018) used borosilicate glass to study mixing efficiency of microfluidic Venturi mixer and microfluidic spiral mixer. Both microfluidic devices were fabricated entirely from borosilicate glass for micro-PIV flow characterization. The micro-channels were developed using wet etching method with depth of 45 μm , incorporating 50 μm thick masking layer of positive photoresist. Photolithography process was employed to create a pattern on the masking layer and acetone was used to remove the layer after etching process was done. Inlet and outlet holes were formed using precise mill-drill system in the top substrate. Top and bottom substrates were permanently sealed by means of fusion thermal bonding process at 650 $^{\circ}\text{C}$.

2.7 Conclusion

Mixing performance is commonly evaluated as a function of mixing index based on homogeneity of the mixing fluids. Considering low mixing performance of microfluidic devices, a number of active and passive mixing mechanisms was discussed to overcome unfavourable laminar flow. Although active micromixers have relatively higher mixing performance, their fabrication process is inherently complex requiring integration of additional actuating components.

CHAPTER 3

METHODOLOGY

3.1 Introduction

This chapter discusses fabrication process and a new method of calculating mixing index for analysing mixing efficiency of the fabricated micromixer. In overall, the methodology adopted in this study is shown in Figure 3.1.

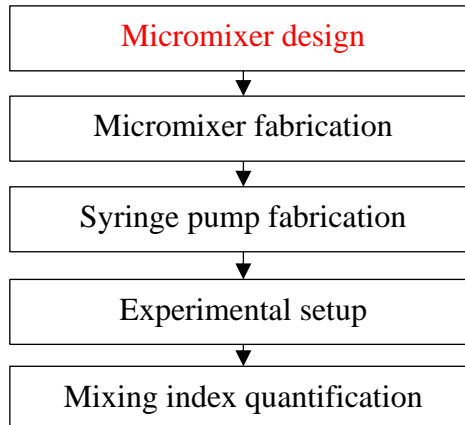


Figure 3.1: Methodology for Micromixers Investigation

Three selected micromixers designs, namely T-, Y- and Dean micromixers were laser fabricated. These designs were selected to study the effects of different mixing junctions and operating conditions towards mixing efficiency. Furthermore, utilization of syringe pump as the fluid driving mechanism is necessary in order to obtain specific Reynolds number during investigation. Proper experimental setup and new mixing quantification method were developed to measure mixing efficiency of different micromixer configurations accordingly. The following section discusses fabrication of the microfluidic devices.

3.2 Design of Microfluidic Device and Fabrication

Micromixers with three different inlet designs, namely T-, Y- and Dean micromixers are shown in Figure 3.2. The Dean micromixer was designed based on unbalanced Dean numbers due to different radius of curvature (Equation 2.4) for both inlets.

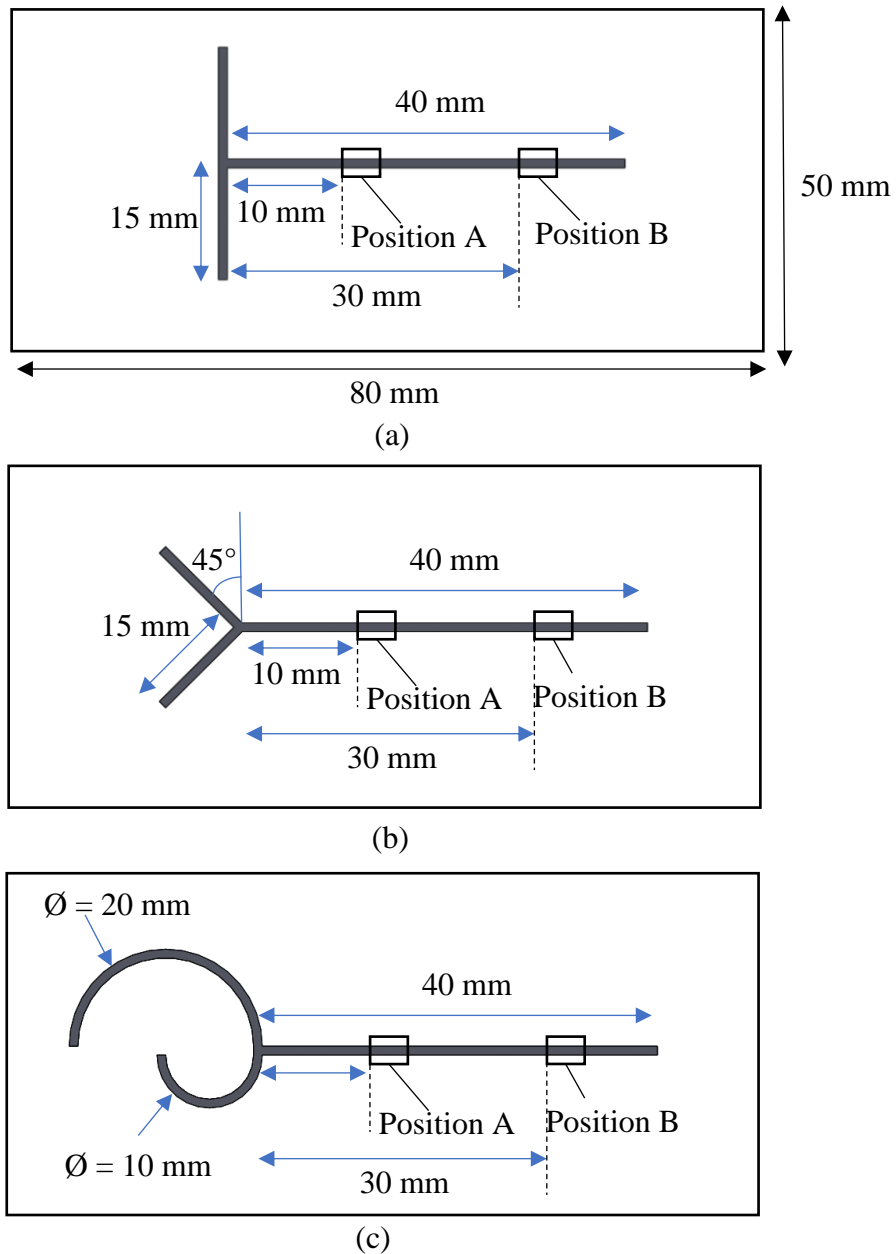


Figure 3.2: Micromixer Designs and Measurement Points (Position A and B)
(a) T-Micromixer (b) Y-Micromixer (c) Dean Micromixer

Ansari et al. (2010) reported that micromixer with Dean number ratio of 1.414 on the basis of split and recombination significantly increases the mixing performance. Instead of varying the widths of split and recombined microchannels as presented in Ansari et al. (2010), the microchannel inlets' radius of curvature was manipulated to achieve similar Dean number ratio. Mixing performance of the Dean micromixer was compared with T- and Y- micromixers as these two micromixers are often employed for benchmarking purposes (Chen et al., 2016b; Faryadi et al., 2014; Karthikeyan & Sujatha, 2019; Le The et al., 2015; Nimafar et al., 2012; Shah et al., 2019). It is noted that the total mixing length of the micromixers is 40 mm.

The procedure to fabricate both micromixers are illustrated in Figure 3.3. The central part of the micromixer consists of a 200 μm thick lamination film, sandwiched in between double-sided adhesive films (each with thickness of 100 μm). After that, a through cut was performed on the sandwiched film using a 40 W CO₂ laser (Model: Fabool, SmartDIY Inc.), producing microchannels with an average width of 250 μm . The fabricated microchannel required three laser passes at power of 1.2 W, speed of 150 mm/s and focal distance of 50.8 mm. To increase structural rigidity of the micromixer, a 3 mm thick PMMA sheet was firmly clamped to the top of the central part. On the other hand, another lamination film was attached to the bottom part instead of using the PMMA sheet primarily to overcome flatness irregularities of the latter substrate. Before final assembly, two inlets and one outlet ports of 5 mm diameter were laser-cut on that PMMA sheet at 40 W, 500 mm/s, 1 pass. These ports were then connected using 3D printed tube connectors to transparent tubing (3 mm internal diameter), and glued together using UV acrylic resin to prevent any leakage. Figure 3.4 and Figure 3.5 show the fabricated micromixers and leak test conducted for the fabricated T- micromixer using blue solution, respectively.

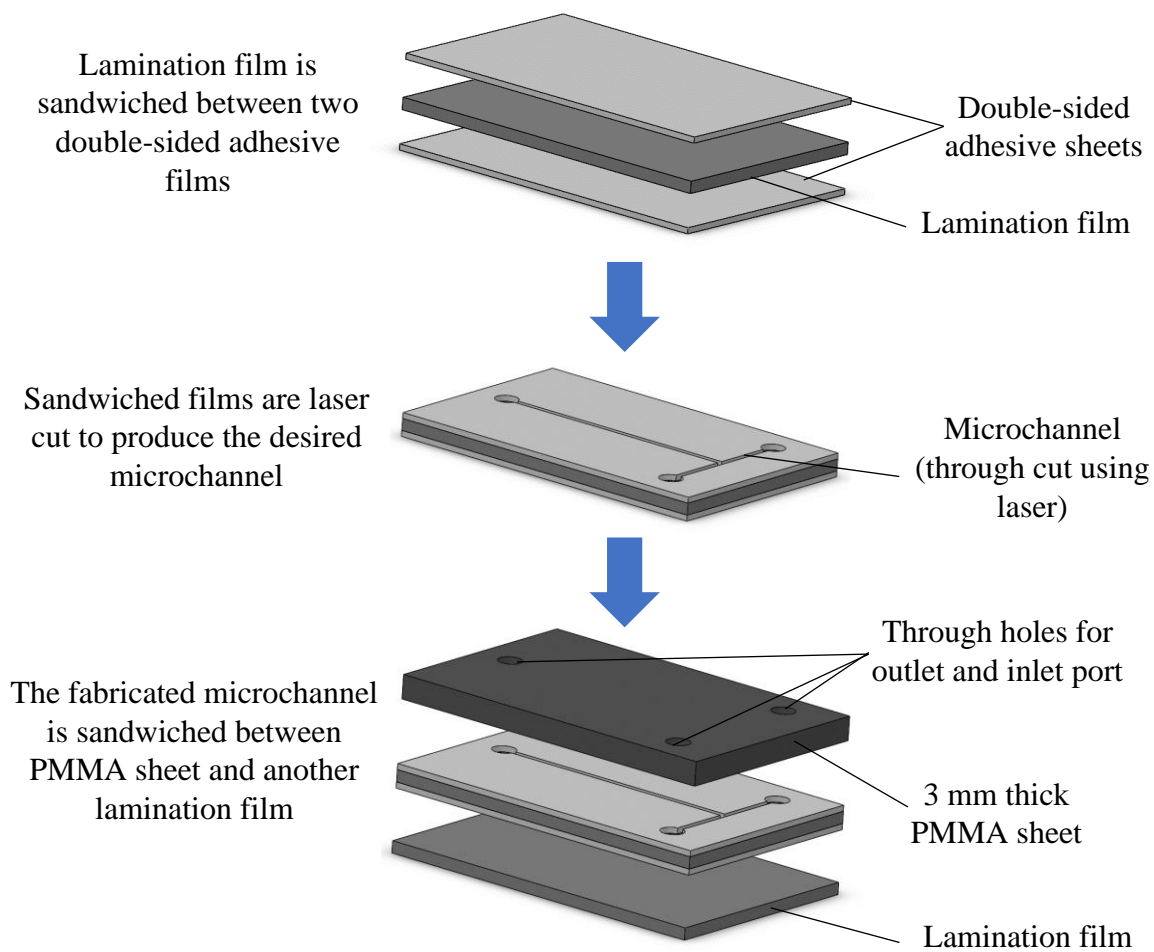


Figure 3.3: Schematic Diagram of the Fabrication Procedure for T-Micromixer

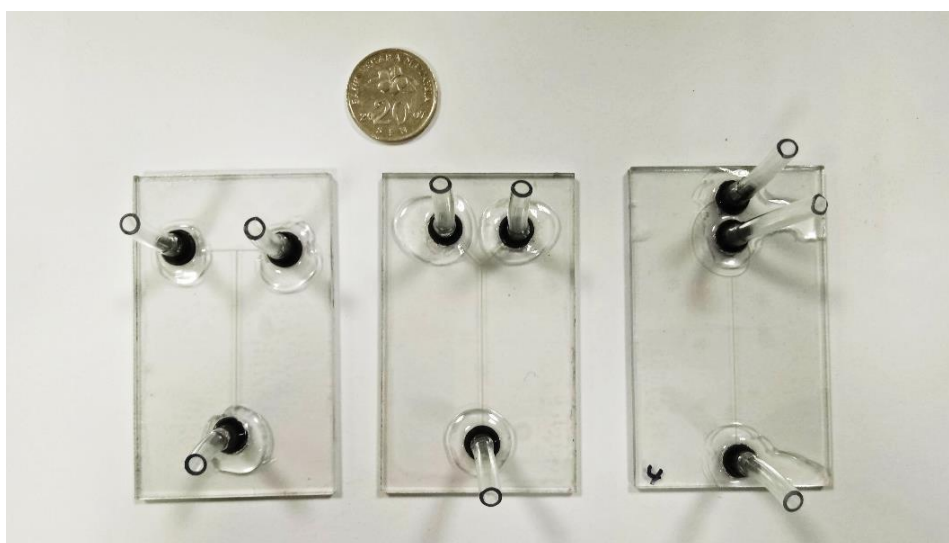


Figure 3.4: Fabricated T-, Y-, and Dean Micromixer

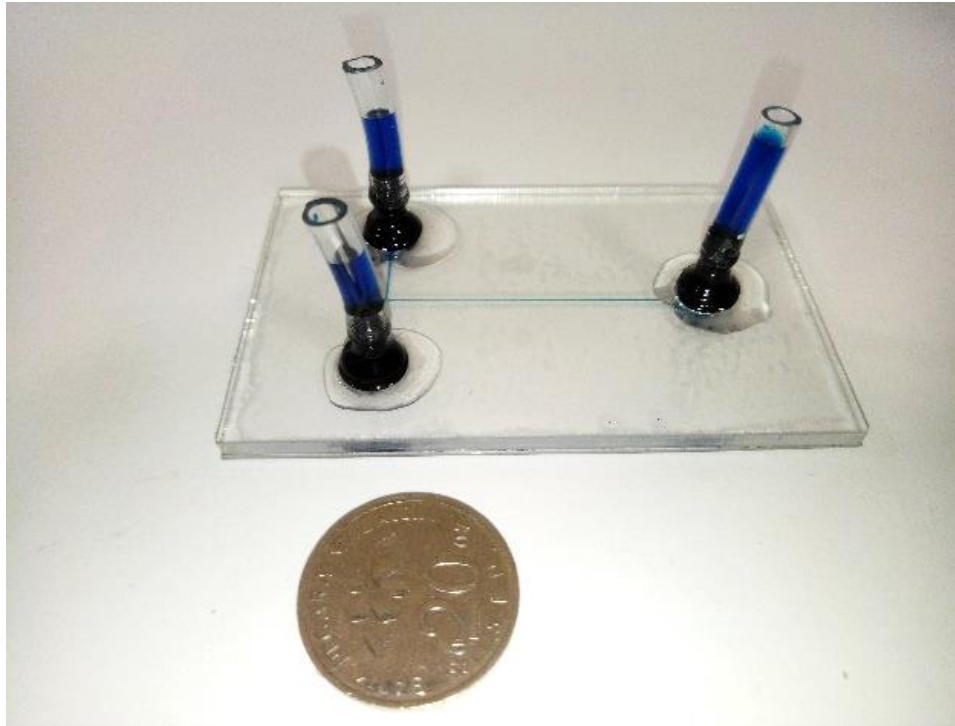


Figure 3.5: Leak Test on T-Micromixer Using Blue Dye

3.3 Syringe Pump Fabrication

Syringe pump was used as the main apparatus for active driving mechanism in microfluidics. Syringe pump is a small positive-displacement pump and has been widely used in this field as the researchers were able to precisely control the operating flow rates. This section explains the mechanism and method adopted to fabricate the syringe pump.

3.3.1 Syringe Pump Mechanism

Figure 3.6(a) shows a general schematic diagram of a syringe pump which comprises of stepper motor, syringe, leadscrew and pusher block. Rotational motion of the motor is transferred to the leadscrew by means of a flexible coupler as shown in Figure 3.6(b). Main mechanism of the syringe pump is the conversion of rotational motion from stepper motor to linear motion of the pusher block. The linear motion of the pusher block is used to drive fluids from the integrated syringe.

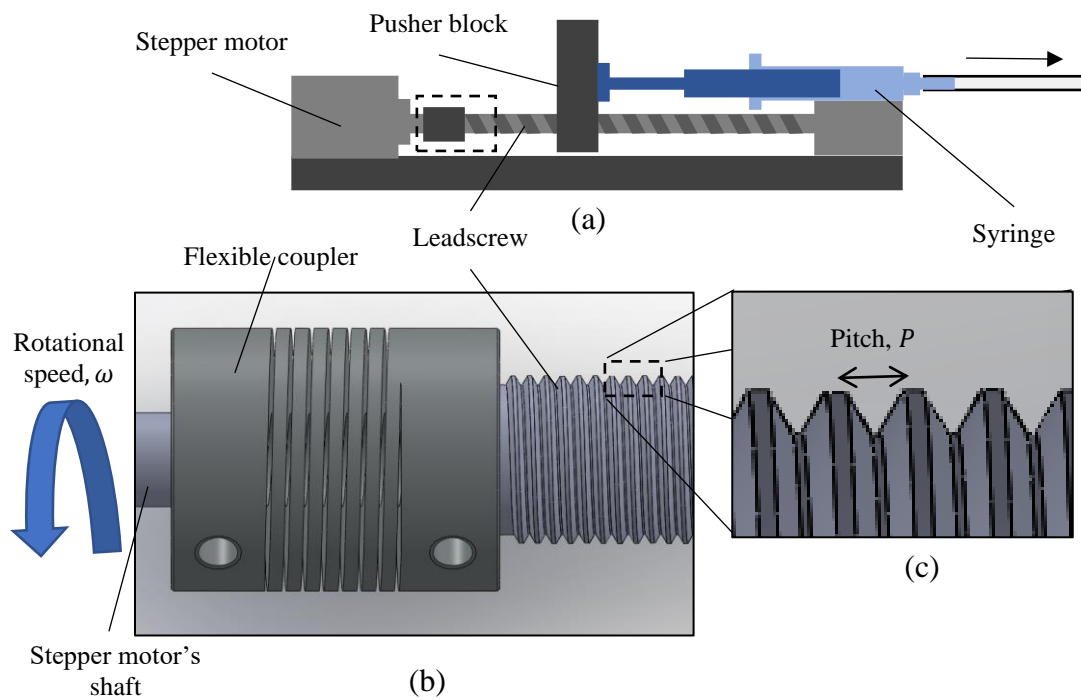


Figure 3.6: Syringe Pump Mechanism (a) Schematic Diagram (b) Assembly of Leadscrew (c) Pitch of Leadscrew

Linear motion of the pusher block in this system can be estimated using angular motion of the motor and pitch distance using Equation 3.1:

$$v_L = P \times \omega \quad \text{Equation 3.1}$$

where v is the system's linear motion velocity (mm/s), P is the pitch distance of the leadscrew (mm) (see Figure 3.6(c)) and ω is angular velocity of the stepper motor (rev/s).

For incompressible and steady flow, law of conservation of mass in a system states that mass flow rate at certain point in the system are the same (Çengel & Cimbala (2019)). Using linear velocity calculated from Equation 3.1, the volume flow rate driven out from the syringe pump can be calculated using Equation 3.2:

$$\dot{V} = A_1 v_1 = A_2 v_2 \quad \text{Equation 3.2}$$

where \dot{V} is volume flow rate of the system, A is the cross-section area at specific point and v is velocity the fluid.

3.3.2 Fabricated Syringe Pump

Figure 3.7 shows a dual syringe pump fabricated in-house using a 3D printer as a means to drive coloured solutions into the microfluidic device. Both syringes are driven by pusher block, connected to a lead screw and actuated by a two-phase stepper motor (NEMA 17) with stepping accuracy of $\pm 5\%$. Two guide rods were used to prevent pusher block from skewing under mechanical loads. The syringe pump is controlled by Arduino Uno microcontroller (see Figure 3.8) and powered by a linear DC power supply (Model: GPS-3030D, Good Will Instrument Co., Ltd). The resolution of the stepper motor used was increased from 200 to 3,200 steps per rotation using A4988 motor driver.

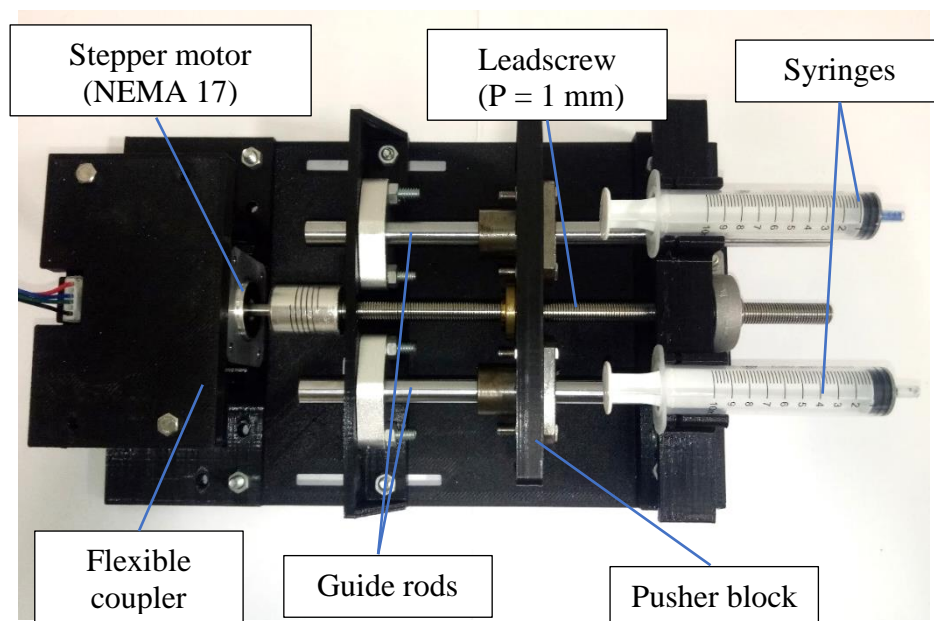


Figure 3.7: Fabricated Syringe Pump

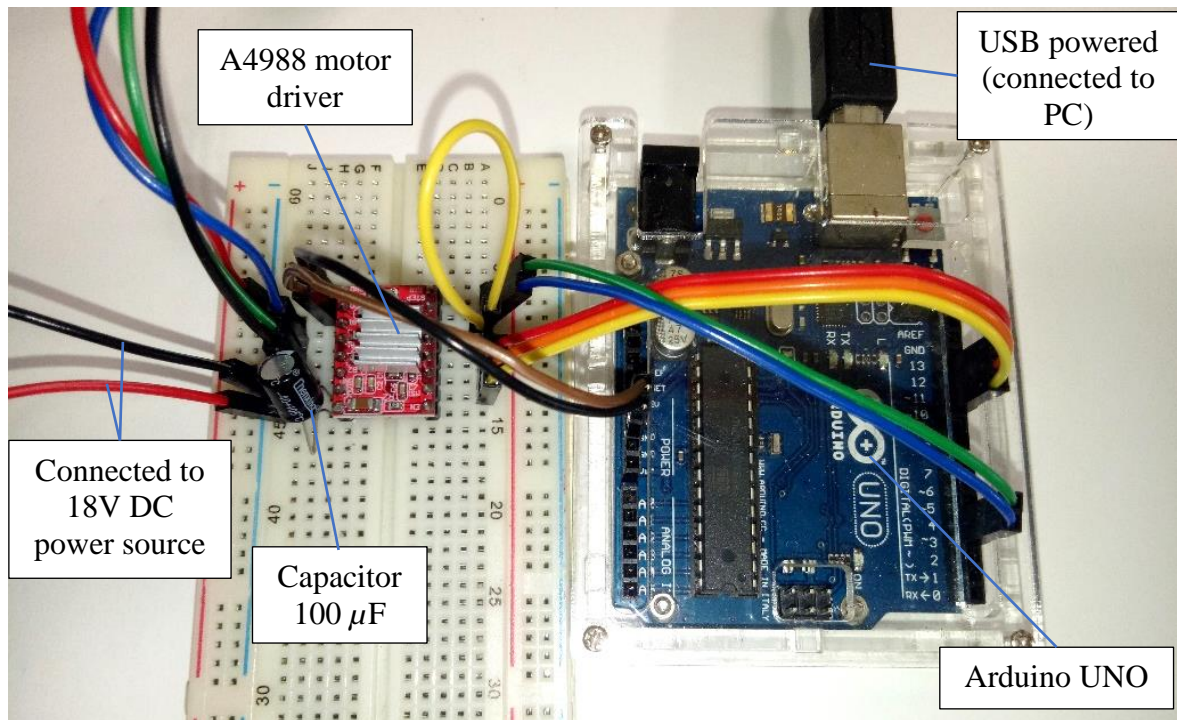


Figure 3.8: Wiring Arrangement for A4988 Motor Driver Connected to Arduino UNO

Syringe pump calibration was performed by comparing theoretical and experimental volume of fluid displaced by the system. Additional precautions were taken by removing bubbles inside the syringe pump and cleaning the lead screw prior to the experiment. Backlash effects were insignificant as reversal motion was only performed after completion of each cycle of the experiment.

Using Equation 3.1 and Equation 3.2, the required speed of the stepper motor to achieve specific Reynolds numbers were computed and listed in Table 3.1. The desired actuating speed was programmed in Arduino Integrated Development Environment (IDE) using C language.

Table 3.1: Stepper Motor Speed for Specific Reynolds Number

Re	Angular velocity (°/sec)	Stepper motor speed (steps/sec)
5	1.47	13
10	2.94	26
20	5.88	52
40	11.77	105
60	17.65	157
80	23.53	209
100	29.42	261

3.4 Experimental Setup

This section discusses the experimental setup used to study mixing index of several micromixers under different operating conditions. As shown in Figure 3.9, the setup comprises of fluid driving mechanism, micromixer, optical imaging system, vibration and heat source.

A dual syringe pump was fabricated in-house using a 3D printer as a means to drive two streams of coloured solutions into the separate inlet arms of T-, Y- and Dean micromixers at an equal flow rate. These coloured solutions; specifically, blue and yellow solutions were produced by diluting food grade dyes into deionized water with ratio of 1:25. The density and viscosity of the coloured solutions are assumed to be similar to those of deionized water.

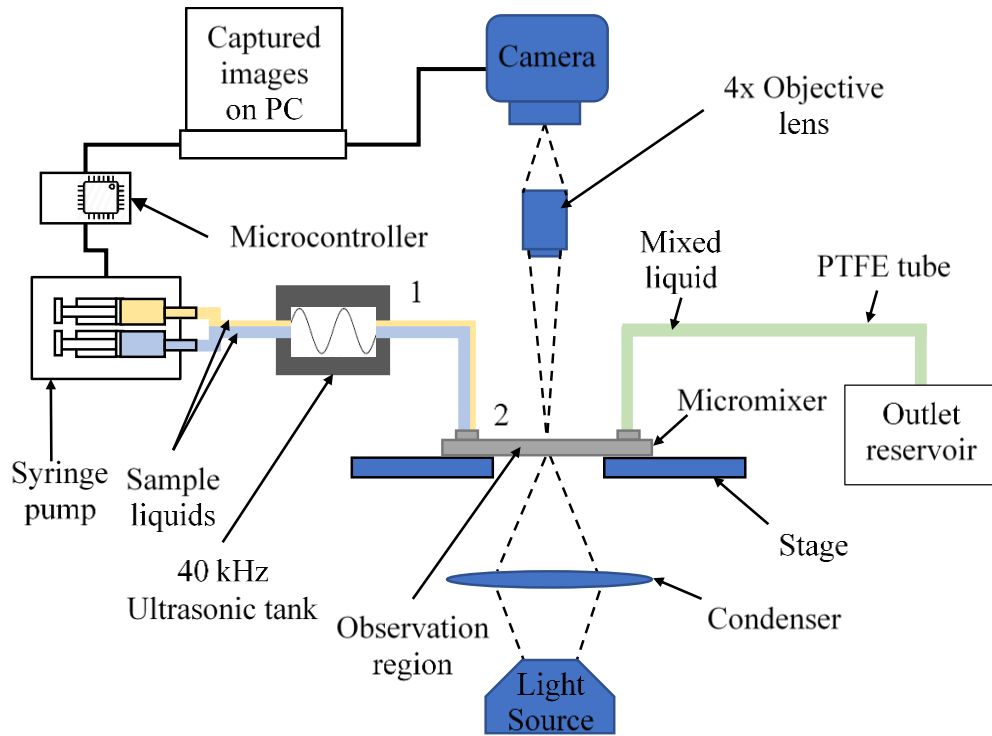


Figure 3.9: Schematic Diagram of the Micromixing Experiment

Both syringes were connected to a lead screw actuated by a two-phase stepper motor (NEMA 17). A compound 5 MP digital video microscope (Model: 40X-2500X LED, AmScope) and 4× magnification was used to capture the images. The microscope has an integrated daylight-balanced LED white light for illuminating the micromixer from the bottom side. It is noted the microscope settings and ambient light were kept constant throughout each experiment. Mixing images were captured using AmScope software prior to post-processing of the images for mixing index quantification utilising built-in functions in MATLAB software. The experimental setup is shown in Figure 3.10.

For a meaningful comparison, the fluid flow inside the micromixer were varied between $5 \leq Re \leq 100$. Two measurement points were selected at which mixing indices were calculated for comparison purposes, as shown in Figure 3.2. According to experimental setup presented, three sets of experiment were conducted which includes validation of proposed

mixing index quantification method (the method was further discussed in Section 3.5), comparison between T-, Y- and Dean micromixers and investigation of extraneously induced ultrasound and thermal effects towards mixing performance.

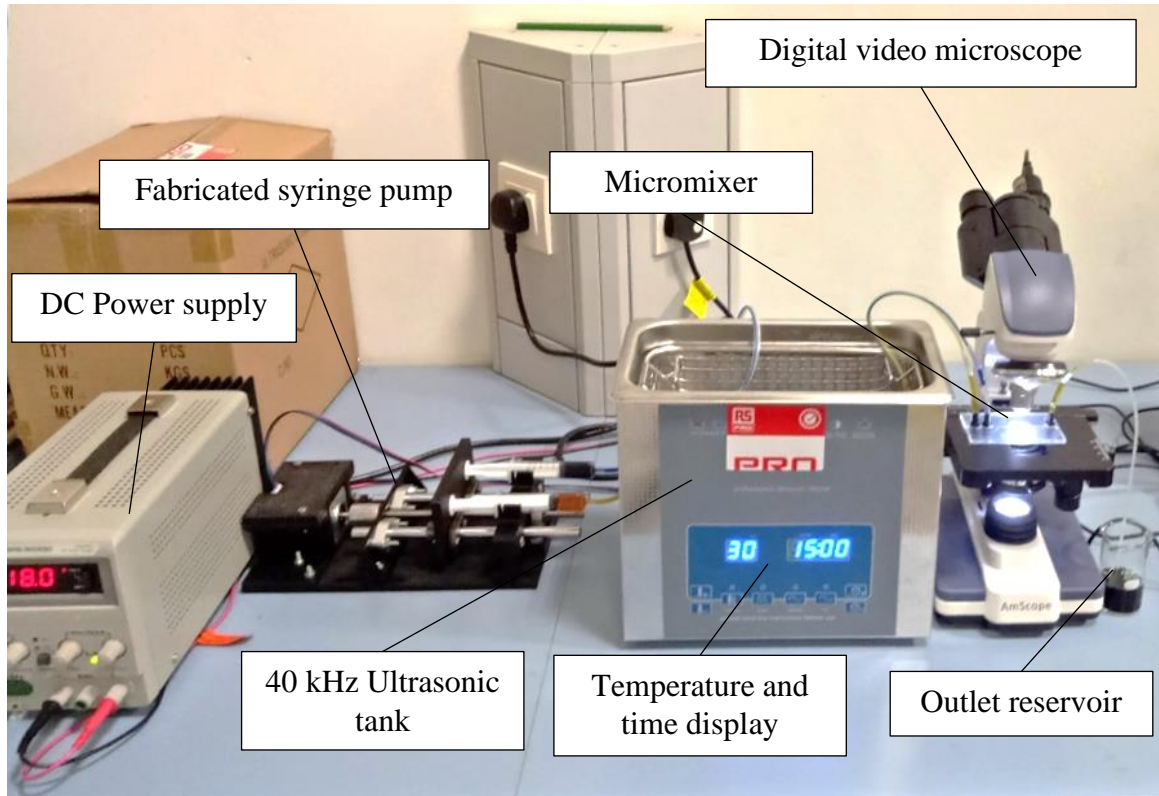


Figure 3.10: Experimental Setup of the Micromixing Experiment

3.4.1 Methods for Validation of Proposed Mixing Index Quantification

In order to validate the proposed method, some experiments were conducted to increase sensitivity and accuracy of the method, and later benchmarked with three common methods used to measure mixing index (Equation 2.7, Equation 2.10 and Equation 2.13) using digital composite images (collages) at predefined mixing indices. Then, well-known T- and Y-micromixers were used to demonstrate the practicality of the proposed method in quantifying the mixing indices. T- and Y-micromixers were used because of their well-

known mixing trend from previous literature. It is noted that the validation of the proposed method was conducted without ultrasound and thermal effects.

3.4.2 Mixing Performance of T-, Y- and Dean Micromixers

Similar to the validation of the proposed method, mixing performance of T-, Y- and Dean micromixers were also evaluated without ultrasound and thermal effects. The mixing index of Dean micromixer which implements unbalanced Dean number at both inlets were compared with the T- and Y- micromixers. The mixing performance of these micromixers were evaluated based on qualitative and quantitative results.

3.4.3 Extraneously Induced Ultrasound and Thermal Energy

To investigate the effect of different operating conditions such as the presence of ultrasonic wave within the microfluidics system towards the mixing index, experiments were carried out by immersing 40 cm PVC tubes at upstream into the activated 40 kHz Ultrasonic tank (Model: SHE-UT8031-EUK, RS Components Ltd.). Additionally, heating element inside the same vibration tank was used to investigate the effect of thermal energy on the sonicated fluids towards the mixing performance. It is noted that the length of tube from position 1 to 2 (see Figure 3.9) was set to be 15 cm.

3.5 Mixing Index Quantification

As mentioned in Section 2.5, conventional mixing index quantification methods for characterizing mixing performance were based on dispersion (homogeneity) information and averaged RGB values, and found leading to either overestimated or underestimated mixing index. To improve the reliability of the estimated mixing index, a straightforward digital image processing method is proposed in this study. Taking into consideration individual RGB values, a theoretical background of the proposed method is discussed in this

section. Experiment were conducted to increase sensitivity and accuracy of the method, and later benchmarked with Equation 2.7, Equation 2.10 and Equation 2.13 using digital composite images (collages). Two well-known T- and Y-micromixers were analysed to demonstrate the practicality of the method in quantifying the mixing indices. Once validated, the proposed method was used to compare the passive mixing performance of different micromixers namely T-, Y- and Dean micromixers. Apart from that, the effects of vibration and heat towards mixing performance were also studied.

3.5.1 Theory of the Proposed Method

To demonstrate the application of this proposed method, Figure 3.11 illustrates three dissimilar fluids coming from different inlets undergoing two-stage mixing in a hypothetically long microchannel within laminar regime. In the first stage, mixing of three solutions, as represented by primary colours (yellow, blue, red) would result in the formation of separate green and purple solutions. The subsequent stage of mixing would eventually produce brown solution. It is known that each of these colours are represented by a set of coded individual RGB values. Here, MATLAB software was used to decode the respective RGB values for each pixel of the mixed and unmixed solutions (see Figure 3.12(a)). Their maximum and minimum RGB values vary which depend on external factors i.e., ambient light and optical properties of the microfluidic substrates.

Accordingly, as shown in Figure 3.12(b), the mixing index can be quantified using the following equation:

$$\text{Mixing Index} = \frac{N_{mixed}}{N_{mixed} + N_{unmixed}} \quad \text{Equation 3.3}$$

where N_{mixed} and $N_{unmixed}$ are the number of pixels classified as mixed and unmixed, respectively, based on the following equations:

$$N_{mixed} = n \left(\{r_{g,min} \leq R \leq r_{g,max} \cap g_{g,min} \leq G \leq g_{g,max} \cap b_{g,min} \leq B \leq b_{g,max}\} \right) \quad \text{Equation 3.4}$$

and

$$N_{unmixed} = n \left(\{r_{b,min} \leq R \leq r_{b,max} \cap g_{b,min} \leq G \leq g_{b,max} \cap b_{b,min} \leq B \leq b_{b,max}\} \right) \quad \text{Equation 3.5}$$

$$+ n \left(\{r_{y,min} \leq R \leq r_{y,max} \cap g_{y,min} \leq G \leq g_{y,max} \cap b_{y,min} \leq B \leq b_{y,max}\} \right)$$

where n is the number of pixels satisfying the prescribed RGB conditions, \cap is the AND Boolean operator. Letters r , g and b respectively denote the red, green and blue values extracted from images. Subscripts g , b and y denote minimum or maximum RGB values of green, blue and yellow pixel, respectively.

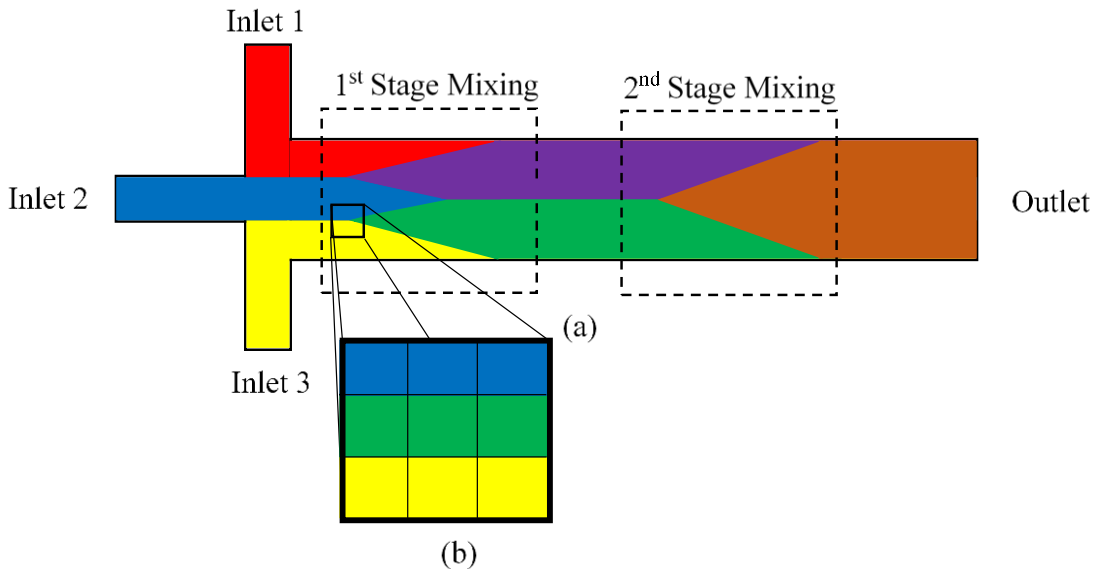


Figure 3.11: Mixing of Three Dissimilar Fluids Coming from Three Separate Inlets (a) Representation of the Fluids Using Different Colours, and (b) Extracted Pixels From the 1st Stage Mixing

For the case shown in Figure 3.12(b), $N_{unmixed}$ consists of both blue and yellow pixels while N_{mixed} is strictly green pixels. The theoretical mixing index of the example discussed is simply 33.3 %. It is noted that this method can be also employed to measure the mixing index for the 2nd stage (see Figure 3.11(a)) by computing the number of brown pixels with respect to total number of brown, purple and green pixels.

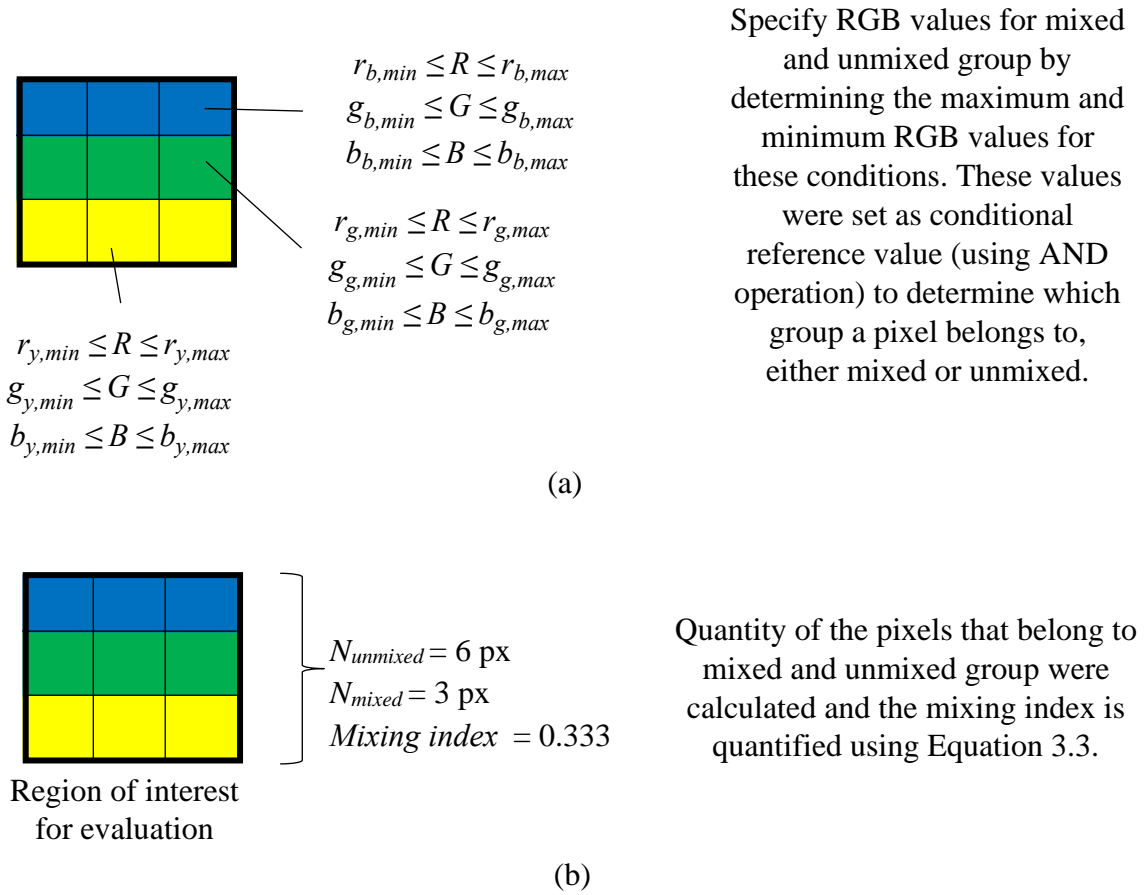


Figure 3.12: Overview of the Proposed Method (a) Specifying the Condition for Each Group Colour (b) Evaluating and Quantifying the Mixing Index

3.5.2 Sensitivity Enhancement for the Proposed Method

As discussed in the preceding section, it is necessary to determine both the maximum and minimum RGB values before calculating the mixing index. These values depend on concentration level of the mixed solution which in turn influenced by rate of mixing. This

rate of mixing predominantly depends on microfluidics geometry, resulting in (transitional) regions having concentrations lesser than 100 %, as illustrated in Figure 3.13. The RGB values before sensitivity enhancement for concentration of 100 % are given in Table 3.1. To include these transitional regions into the mixing index calculation, sensitivity enhancement of the RGB model was proposed.

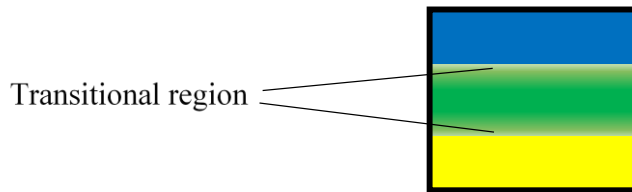


Figure 3.13: Illustration of the Transitional Region

Initially, a premixed green solution was prepared by manually mixing 1 mL blue and 1 mL yellow dyes with 50 mL deionized water. By adding 2 mL of deionized water to 10 mL of the premixed green solution, the concentration reduces to 83.3 %. A similar step was taken to gradually produce different concentration levels (71.4 %, 62.5 %, 55.6 %, 50.0 %, 45.5 % and 41.7 %), each providing a new set of RGB values. In practice, having concentration down to 0% (purely deionized water) is not possible. It is noted that this dilution method is suitable especially for fluids flowing at equal flow rate. In some cases where two dissimilar fluids flowing at different flow rates for the same T- and Y- micromixers (Faryadi et al., 2014) or mixing occurring in microchannel with irregular geometries (Chen et al., 2016b); different preparation methods may be required by pre-mixing them in different proportions.

To demonstrate the effects of further dilution (reduced fluid concentration) on mixing index, mixing indices of T-micromixer at $Re = 5, 10$ and 20 for different concentrations are

given in Figure 3.14. It shows that the mixing index remains constant once the concentration reaches 50 % irrespective of different Reynolds number. In other words, increasing the upper limits of the RGB by reducing the concentration from 50 % ($20 \leq R \leq 92$, $80 \leq G \leq 125$, $23 \leq B \leq 105$) to 41.7 % ($20 \leq R \leq 96$, $80 \leq G \leq 129$, $23 \leq B \leq 116$) does not have any effect on the calculated mixing index.

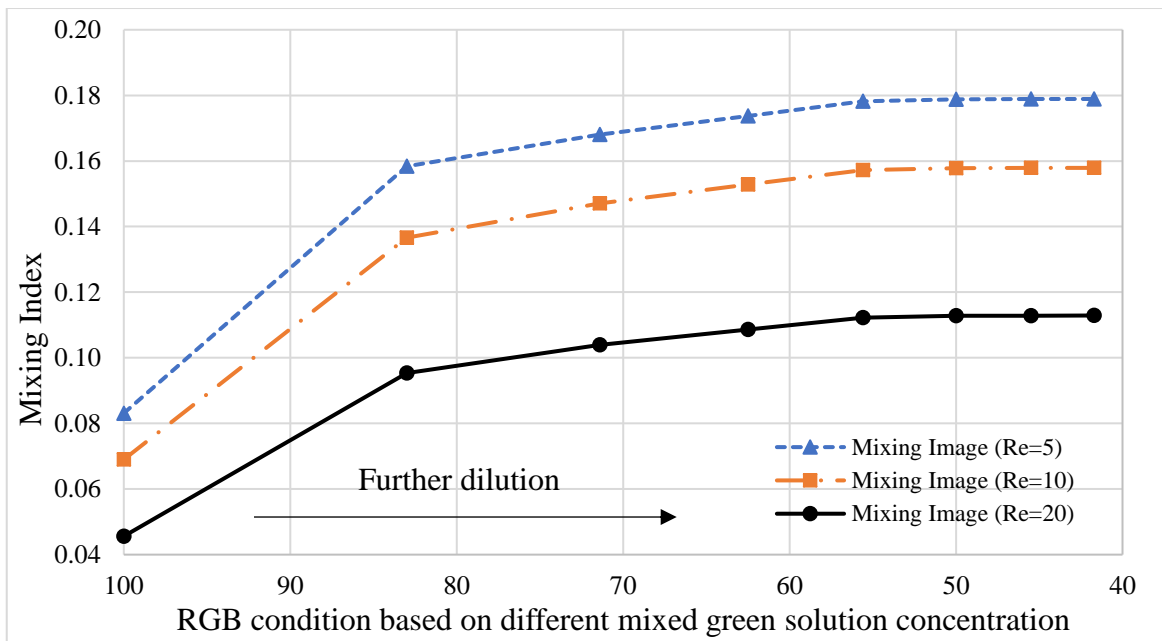


Figure 3.14: Effects of Sensitivity Enhancement on Calculated Mixing Index

3.5.3 RGB Values After Sensitivity Enhancement

As shown in Figure 3.15, it is noted that further dilution would increase the upper limits of each RGB values, which in turn would increase the mixing index. Each diluted green concentration exhibits different ranges of RGB values. For example, green solution of 50 % concentration can be easily identified having $59 \leq R \leq 92$, $95 \leq G \leq 125$ and $71 \leq B \leq 105$. The new RGB values were taken at the 41.7 % concentration as shown in Figure 3.15 as the further reduction in concentration of the green solution have no change on the mixing index (refer Figure 3.14).

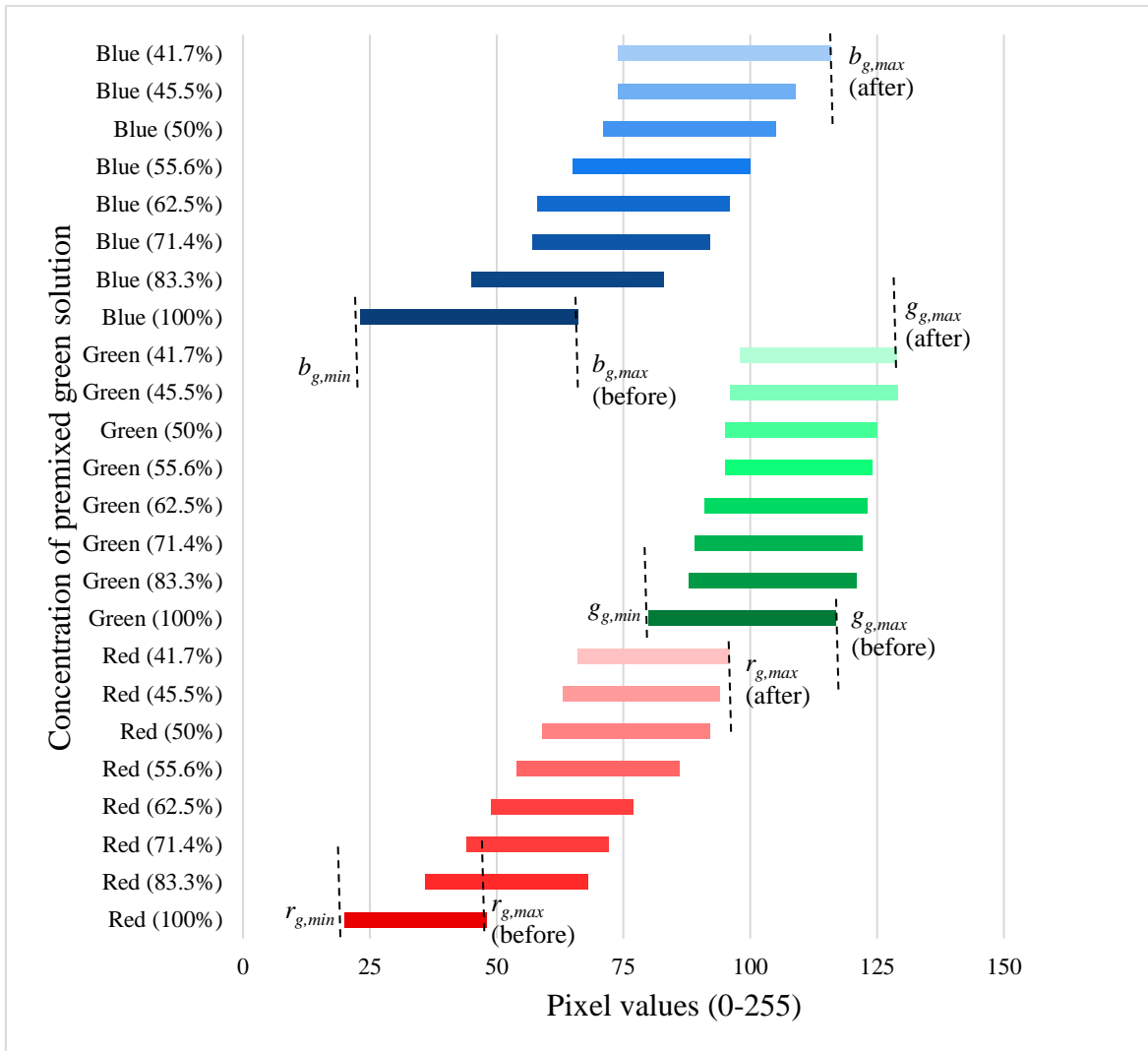


Figure 3.15: RGB Values of Premixed Green Solution at Different Concentration Levels

Based on Figure 3.15, a new set of RGB values for green solution after sensitivity enhancement is listed in Table 3.1. The outcome of the proposed sensitivity enhancement in detecting the transitional region of a randomly chosen actual mixing images is shown in the form of binary image in Figure 3.16. It is apparent that the number of detected green pixels increases after sensitivity enhancement

Table 3.2: Sets of Reference RGB Values for Blue, Yellow and Green Solutions

	Blue solution	Yellow solution	Green solution	
			Before sensitivity enhancement (100 % concentrated)	After sensitivity enhancement
R	$0 \leq R \leq 19$	$59 \leq R \leq 136$	$20 \leq R \leq 48$	$20 \leq R \leq 96$
G	$42 \leq G \leq 100$	$50 \leq G \leq 131$	$80 \leq G \leq 117$	$80 \leq G \leq 129$
B	$50 \leq B \leq 156$	$0 \leq B \leq 8$	$23 \leq B \leq 66$	$23 \leq B \leq 116$

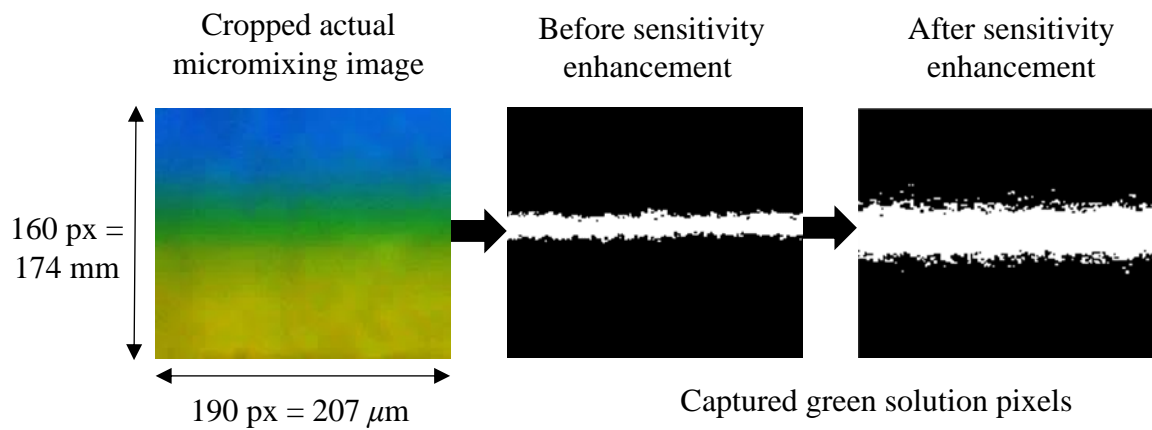


Figure 3.16: Effect of Sensitivity Enhancement on Detecting the Transitional Region

CHAPTER 4






RESULTS AND DISCUSSION

4.1 Validation of Proposed Method using Digital Composite Images

To benchmark the proposed method with others (Equation 2.7, Equation 2.10, and Equation 2.13), a set of composite images at predefined mixing indices (0, 0.5, 1.0) was prepared. As shown in Table 4.1, images of each prepared solutions were cropped to a size of 190×160 pixels. It is evident that the proposed method accurately predicts the mixing index similar to that of the theoretical mixing index. Equation 2.10 produces comparable results for all mixing indices, significantly better than Equation 2.7, and Equation 2.13.

It is noted that results of Equation 2.7, Equation 2.10, and Equation 2.13 show overprediction for mixing index = 0 and underestimation for mixing index = 1 due to the inherent limitation of averaging individual RGB pixel intensities in the form of grayscale and HSI formats. This causes ambiguity in differentiating various coloured solutions. In addition, these equations utilize standard deviation intensity on the basis of dispersion information and homogeneity of the solution (Fu et al., 2017), causing large errors for determining mixing index of both completely mixed and unmixed solutions. In practice, it is not possible to obtain mixing index = 0 and 1 because the normalized pixel intensity (see Equation 2.8 and Equation 2.11) is normally distributed. For this reason, mixing indices for homogenous blue and yellow composite images were overestimated even in the absence of green pixels for the case of mixing index = 0.

Table 4.1: Benchmarking Against Different Mixing Index Calculation Methods Using Digital Composite Images. Each Cropped Image Size is $207 \times 174 \mu\text{m}^2$

Microscopic composite images	Theoretical mixing index	Proposed method (Equation 3.3)	Equation 2.7	Equation 2.10	Equation 2.13
	0	0	0.665	0.042	0.685
	0	0	0.699	0.193	0.718
	0	0	0.289	0.136	0.683
	0.5	0.500	0.403	0.476	0.440
	1.0	1.000	0.731	0.913	0.760

4.2 Benchmarking Against Other Methods using T- and Y-Micromixers

Qualitative images of the experimental results for both T- and Y-micromixers are presented in Table 4.2 and Table 4.3, respectively. It can be observed that a discernible layer of green solution formed along the horizontal direction as the two distinct solutions are gradually mixed. This is because the mixing enhances as the fluids flowing downstream the straight microchannels (from position A to B) (Fu et al., 2017; Lin et al., 2004). Due to the symmetrical nature of the microchannels, the mixing appears to occur largely at the central region of the microchannels at the interface of two fluids, dominantly attributed to diffusive mixing mechanism (Sarkar et al., 2014).

Table 4.2: Actual Mixing Images in T-Micromixer at Different Reynolds Numbers. MI Stands For Mixing Index. Each Cropped Image Size is $250 \times 174 \mu\text{m}^2$





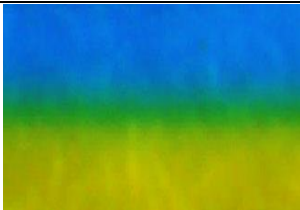
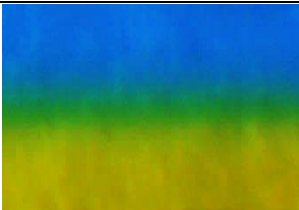




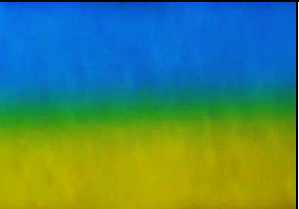

Reynolds number		Re = 5	Re = 40	Re = 100
Mixing images	Position A	 MI = 0.179	 MI = 0.084	 MI = 0.072
	Position B	 MI = 0.350	 MI = 0.127	 MI = 0.106

Table 4.3: Actual Mixing Images in Y-Micromixer at Different Reynolds Numbers. Each Cropped Image Size is $250 \times 174 \mu\text{m}^2$

Reynolds number		Re = 5	Re = 40	Re = 100
Mixing images	Position A			
		MI = 0.157	MI = 0.081	MI = 0.070
	Position B			
		MI = 0.278	MI = 0.112	MI = 0.098

The quantitative results of mixing index at different Reynolds numbers for both micromixers are shown in Figure 4.1. The mixing index in Figure 4.1 was analysed at Position B, which is 30 mm away from the junction. Several points can be drawn from Figure 4.1. Firstly, the experimental result shows similar mixing effect among these two designs because diffusion is the decisive factor in mixing at such low Re (Wang et al., 2012). It is observed the highest mixing efficiency is attainable at the lowest Reynolds number (Re = 5). Secondly, the mixing index of T-micromixer was found better than that of Y-micromixer which agrees well with the findings in (Faryadi et al., 2014; Sarkar et al., 2014). Thirdly, it is obvious that the mixing phenomena of both micromixers enhance with the decrease of Reynolds number, exhibiting similar characteristics with the previous studies (Hong et al., 2004; Matsunaga et al., 2013; Scherr et al., 2012; Yang et al., 2007). This trend is only found

at low Reynolds number ($Re < 150$) where molecular diffusion is dominant and it is expected to increase at $Re > 150$ due to formation of asymmetric regime (Rudyak & Minakov, 2014) and engulfment region (Galletti et al., 2012). The low mixing index at higher Reynolds number is attributed to shorter residence time since the residence time is inversely proportional to the Reynolds number (Matsunaga et al., 2013). In between $40 \leq Re \leq 100$, it can be observed that a marginal reduction in mixing index of the proposed method occurred which lies around the value of 0.1.

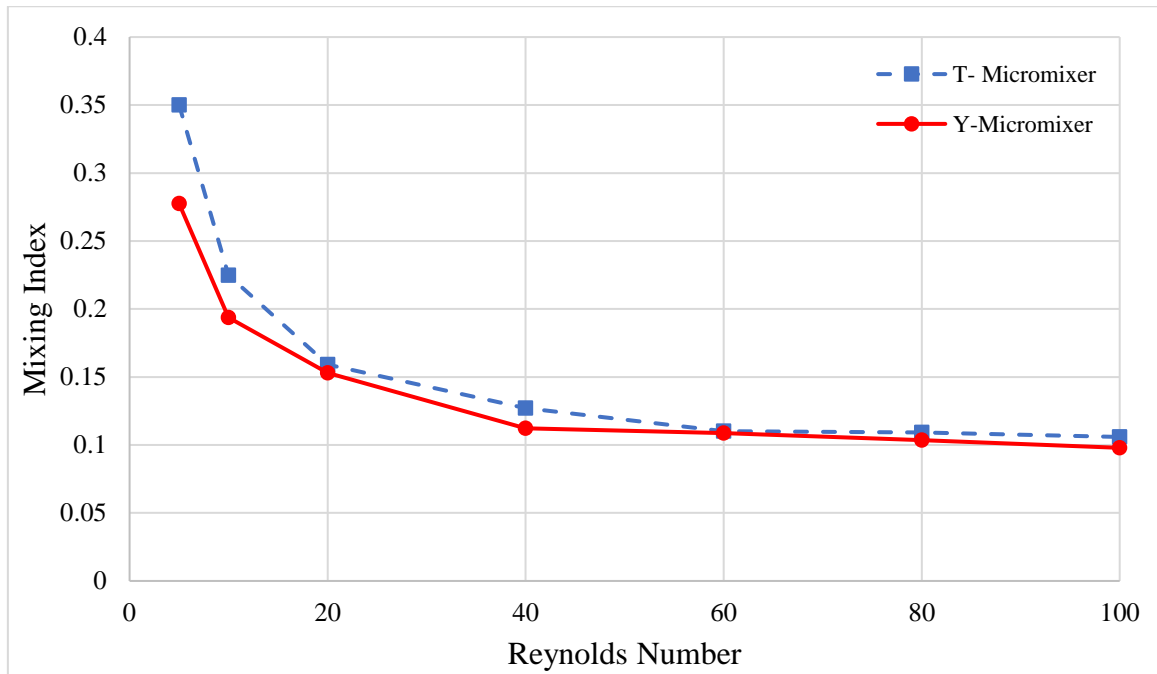


Figure 4.1: Mixing Index of T- and Y-Micromixers at Position B Calculated Using the Proposed Method

Figure 4.2 and Figure 4.3 compare calculated mixing indices using different methods at varying Reynolds numbers. It is clear that the calculated mixing index using Equation 2.10 demonstrates an almost similar monotonic trend to that of the proposed method but with mixing indices reported two times greater than the latter. However, contradicting trends are observed for Equation 2.7 and Equation 2.13. Besides, mixing index calculated from

Equation 2.7, Equation 2.10, and Equation 2.13 shows non-monotonic characteristics for $40 \leq Re \leq 100$. Fu et al. (2017) also reported some discrepancies where non-monotonic characteristics were observed when comparing several mixing index methods. In addition, Equation 2.7, Equation 2.10, and Equation 2.13 tend to overpredict the mixing index especially those at higher Reynolds numbers. This further validates the benchmarking results as shown in Table 4.1. In short, the proposed method (Equation 3.3) provides more reliable results as it used multiple distinctive conditions, i.e., red, green and blue to characterize the mixing instead of a single component of the averaged intensity value.

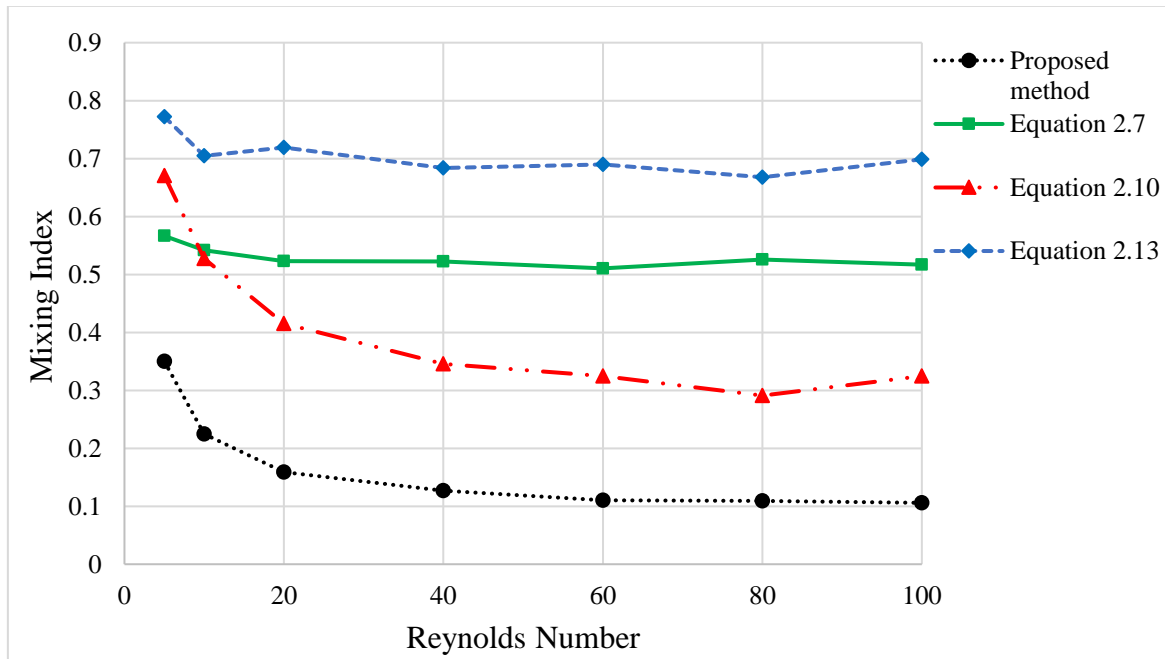


Figure 4.2: Comparison of Calculated Mixing Index in T-Micromixer Against Other Methods

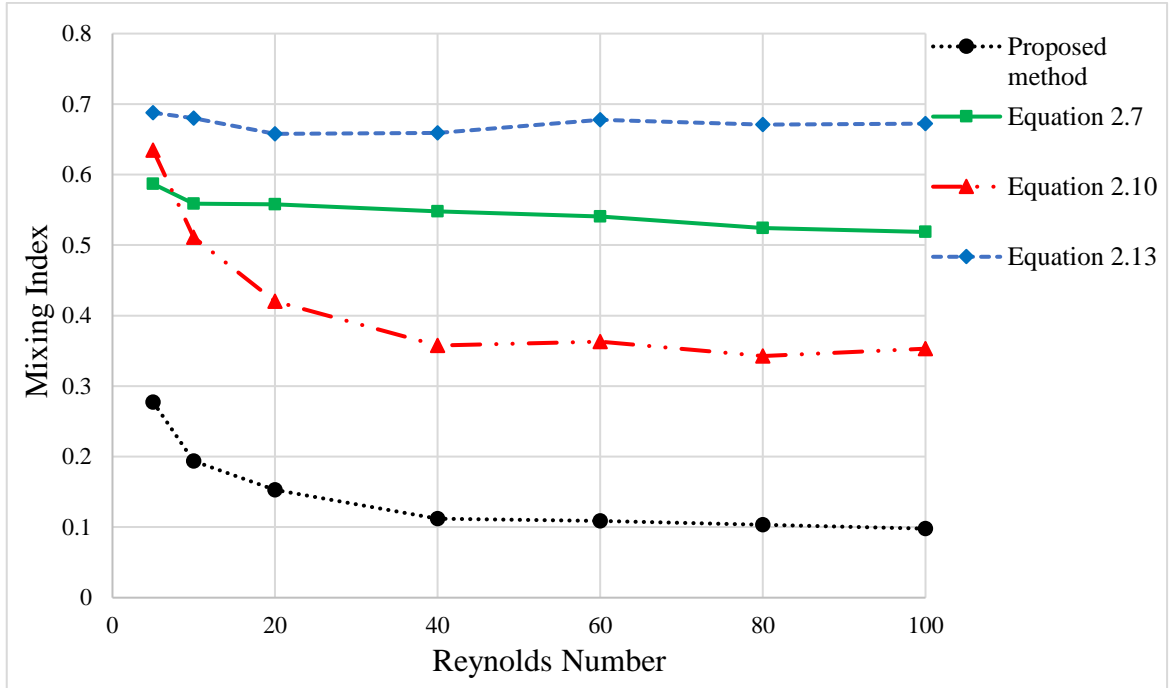


Figure 4.3: Comparison of Calculated Mixing Index in Y-Micromixer Against Other Methods

4.3 Comparison of Mixing Index Between T-, Y- and Dean Micromixers

Qualitative images of the experimental results for T-, Y- and Dean micromixers along the straight microchannels are presented in Table 4.2, Table 4.3 and Table 4.4, respectively. Initially, the two dissimilar fluids undergoing mixing at the junction before flowing into the straight mixing channel. A new passive micromixer based on the concept of unbalanced Dean vortices at the inlet fluid streams has been proposed and fabricated using laser micromachining process. Experimental analysis was performed to compare the mixing index of the T-, Y- and Dean micromixers for Reynolds numbers ranging from 5 to 100.

Table 4.4: Actual Mixing Images in Dean Micromixer at Different Reynolds Numbers. Each Cropped Image Size is $250 \times 174 \mu\text{m}^2$





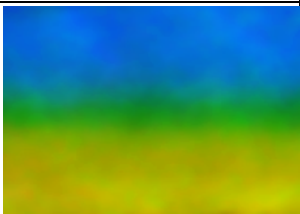

Reynolds number		Re = 5	Re = 40	Re = 100
Mixing images	Position A			
		MI = 0.171	MI = 0.091	MI = 0.076
	Position B			
		MI = 0.331	MI = 0.143	MI = 0.137

Figure 4.4 compares quantitative mixing index of T-, Y- and Dean micromixers at position B for $5 \leq \text{Re} \leq 100$ in the absence of ultrasonic excitation and thermal energy, computed using the proposed method. It is clear a similar mixing trend can be observed irrespective of the inlet geometrical designs where the mixing enhances with the decrease of Reynolds number. All three micromixers show relatively higher mixing index at lower Reynolds number attributed to increased molecular diffusion due to higher residence time (Matsunaga et al., 2013).

It is noted that the T-micromixer demonstrates marginally higher mixing performance as compared to Y- and Dean micromixers for $5 \leq \text{Re} \leq 20$. This is because the effect of molecular diffusion is more pronounced than that of Dean flows. In the curved microchannel (refer Figure 3.2(c)), higher velocity magnitude at the channel centre has the

tendency to move outward of curvature, creating a radial pressure gradient. Because of this centrifugal pressure gradient, the more stagnant fluid near the inward wall would re-circulate to the centre, forming two counter-rotating vortices called Dean vortices with different magnitude depending on the radius of curvatures (Di Carlo, 2009). Hence, fluids originating from two dissimilar geometrical inlets having different Dean numbers causes unbalanced collision of the secondary flow (Dean vortices), and the Dean effect on mixing index becomes more significant at $Re > 20$ (Ansari et al., 2010; Di Carlo, 2009). This agrees well with the earlier study by Shah et al. (2019) who found that the effects of Dean number on mixing is more apparent at higher Reynolds number since Dean number is proportional to Reynolds number (see Equation 2.4). For this reason, the Dean micromixer exhibits higher mixing performance (about 27 % better) as compared to T- and Y- micromixers for $40 \leq Re \leq 100$.

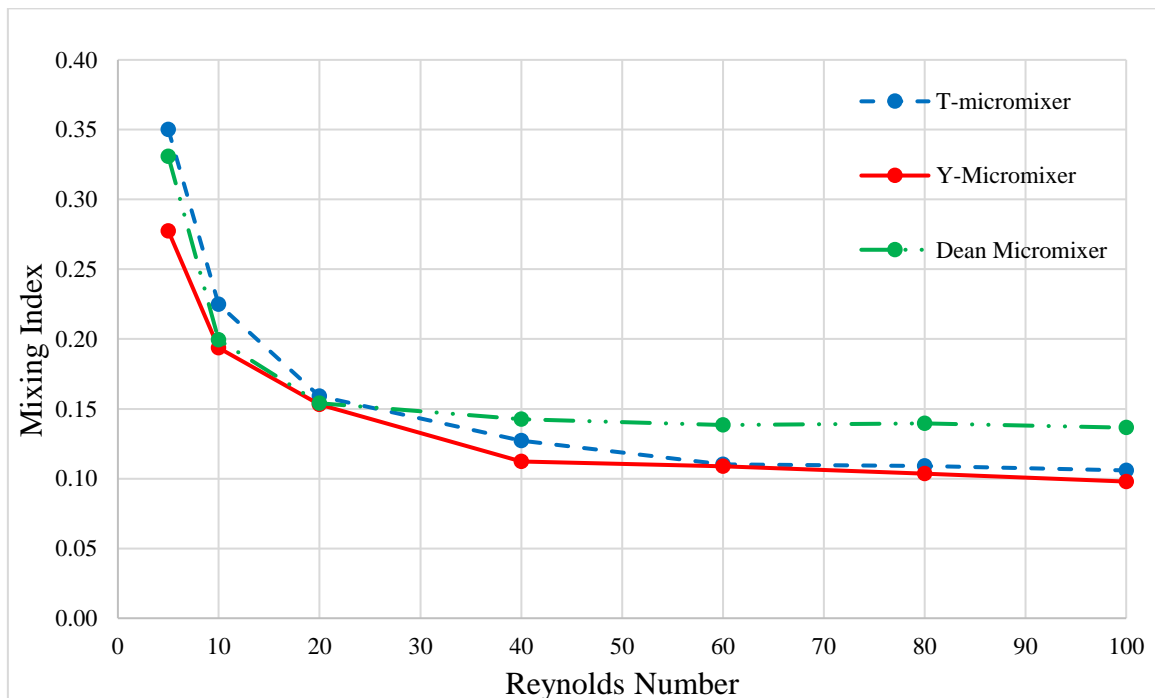


Figure 4.4: Mixing Index of T-, Y- and Dean Micromixer at Position B

4.4 Influence of Extraneously Induced Ultrasound and Thermal Energy on Mixing

In the previous experiment, the working fluid temperature was maintained at 25 °C. However, ultrasonic wave propagation within the fluid would result in temperature rise of the fluid (Seip & Ebbini, 1995), and therefore the fluid temperature was maintained at 30 °C for determining the sole effect of ultrasound towards mixing index. The combined ultrasound and thermal effects were subsequently studied at temperature of 60 °C. Such a higher temperature than normal room conditions is necessary for some processes i.e., micromixing and subsequent polymerase chain reaction for influenza viral DNA fragment (Kim et al., 2009) and loop mediated isothermal amplification on a microfluidic platform for foodborne pathogen detection (Sayad et al., 2016). It is assumed negligible losses of ultrasound energy and heat energy as the fluid moving from the source to the interrogation point. Qualitative images of the experimental results for Dean micromixers subjected to 40 kHz ultrasound at 30 °C and 60 °C are presented in Table 4.5 and Table 4.6, respectively. The Dean micromixer was used here to investigate the effects of ultrasound and thermal energy as it has been demonstrated earlier performing better at higher Reynolds number ($Re > 20$), as shown in Figure 4.4. Such a comparison is necessary above this Reynolds number since the micromixing is more efficient in terms of operating time and mixing performance. It is expected that T- and Y- micromixers would demonstrate similar trends and therefore not investigated further.

Table 4.5: Actual Mixing Images in Dean Micromixer for 40 kHz Ultrasound and 30 °C at Different Reynolds Numbers. Each Cropped Image Size is $250 \times 174 \mu\text{m}^2$








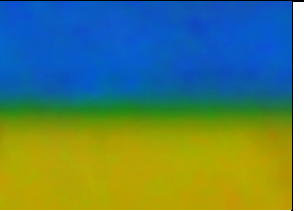
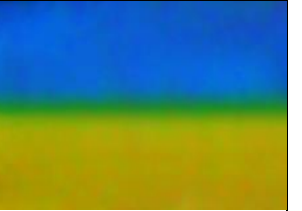



Reynolds number		Re = 5	Re = 40	Re = 100
Mixing images	Position A	 MI = 0.207	 MI = 0.095	 MI = 0.078
	Position B	 MI = 0.453	 MI = 0.173	 MI = 0.145

Table 4.6: Actual Mixing Images in Dean Micromixer for 40 kHz Ultrasound and 60 °C at Different Reynolds Numbers. Each Cropped Image Size is $250 \times 174 \mu\text{m}^2$

Reynolds number		Re = 5	Re = 40	Re = 100
Mixing images	Position A	 MI = 0.233	 MI = 0.099	 MI = 0.080
	Position B	 MI = 0.493	 MI = 0.186	 MI = 0.156

The results of mixing index at different operating conditions for the Dean micromixer are shown in Figure 4.5, where the mixing index decreases with the increase of Reynolds number. The highest mixing index for varying Reynolds number ($5 \leq Re \leq 100$) can be attained under the influence of both ultrasound and thermal energies and followed by ultrasound energy only. This can be attributed to formation of strong micro-streams and micro-jets induced by the collapse of microbubbles due to cavitation generated by the ultrasonic wave propagation (sonication) (Parvizian et al., 2011). Furthermore, absorption of acoustic energy during the passage of acoustic wave results in energy gradient that induces macroscopic and convective flows through the liquid causing a phenomenon called acoustic streaming (Faryadi et al., 2014; Sutkar & Gogate, 2010). Acoustic streaming is favourable as it enhances micromixing by providing micro agitation inside the liquid phase (Parvizian et al., 2011; Rahimi et al., 2013). Additionally, temperature rise reduces fluids viscosity allowing the Dean vortices to retain their hydrodynamic identity longer for enhanced molecular diffusion (Parvizian et al., 2011).

It can be observed that the ultrasound and thermal effects towards mixing performance is more significant at $5 \leq Re \leq 20$ because of increased residence time (Faryadi et al., 2014; Xu et al., 2011). Due to increased residence time, the external energies transmitted which were responsible for mechanical effect within the system are prolonged, increasing mass transfer between these mixing fluids (Rahimi et al., 2013). It is also found that the mixing index increases of about 6 % to 10 % at various Reynolds number once the sonicated mixing fluids were heated from 30 °C to 60 °C.

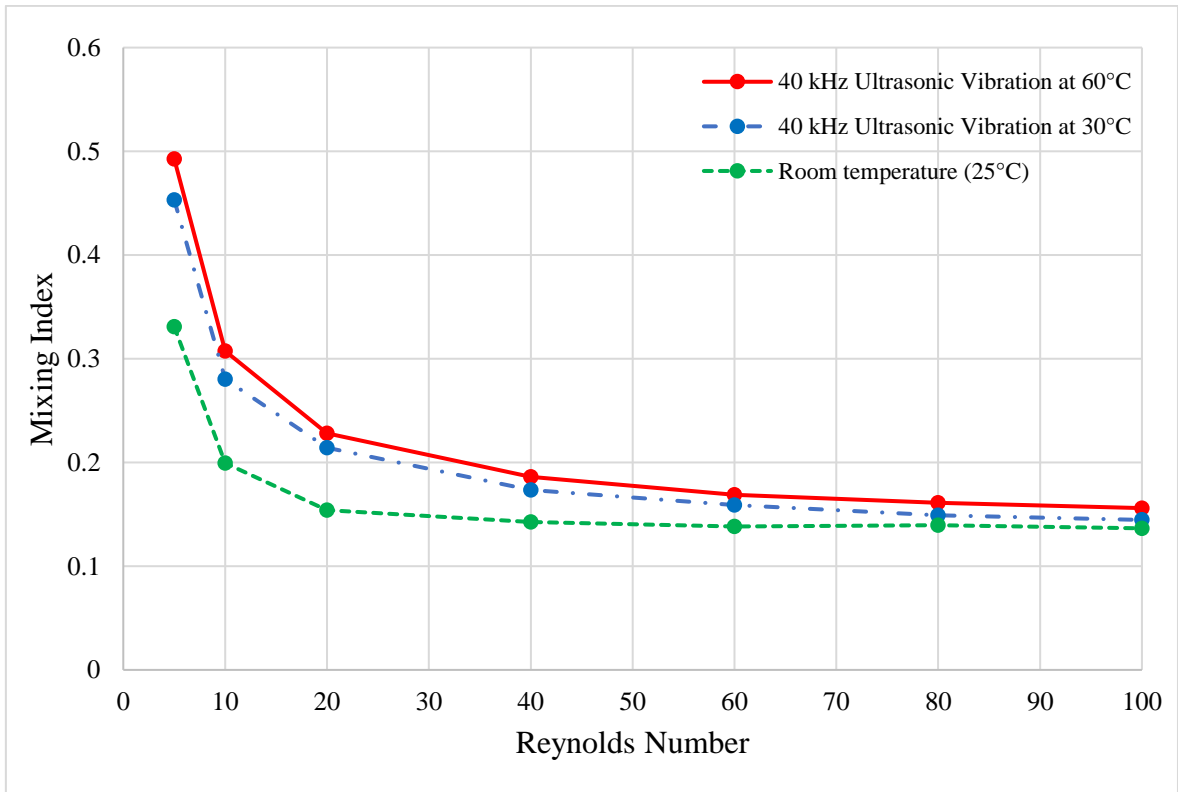


Figure 4.5: Mixing Index of Dean Micromixer for Different Operating Conditions at Position B (30 mm Downstream From the Junction)

CHAPTER 5

CONCLUSION AND RECOMMENDATIONS

5.1 Conclusion

Micromixing is principally crucial in many microfluidics applications. Mixing index or mixing performance is a paramount criterion in determining the micromixing effect which is typically performed using dispersion information. The primary limitation of the methods is that the individual RGB values are first averaged before mixing index is computed. In this study, a new method utilizing RGB colour model to characterize mixing performance was presented. In comparison with other methods, the enhanced RGB model was successfully tested through evaluation of digital composite images. Furthermore, the practicality of this proposed method was demonstrated through mixing experiment of T- and Y-micromixer at varying Reynolds numbers. Results show mixing index decreases with the increase of Reynolds number. The mixing index of T-micromixer was found better than that of Y-micromixer which agrees well with the literature. This method was successfully proven overcoming the limitation of previous methods which overestimated or underestimated the calculated mixing index.

In comparison, the Dean micromixer exhibits higher mixing performance (about 27 % better) as compared to T- and Y- micromixers for $40 \leq Re \leq 100$, as the Dean effect is more significant at higher Reynolds number. Furthermore, the highest mixing index for varying Reynolds number ($5 \leq Re \leq 100$) can be attained under the influence of both ultrasound and thermal energies. This can be attributed to formation of strong micro-streams and micro-jets induced by the collapse of microbubbles due to cavitation generated by the ultrasonic wave propagation (sonication). It can be observed that the ultrasound and thermal

effects towards mixing performance are more significant at $5 \leq Re \leq 20$ because of prolonged mechanical effect within the system. It is also found that the mixing index increases of about 6 % to 10 % at various Reynolds number once the sonicated mixing fluids were heated to 60 °C. The temperature rise reduces fluids viscosity, allowing the Dean vortices to retain their hydrodynamic identity longer for enhanced molecular diffusion.

5.2 Recommendations

It is suggested that the proposed method based on RGB model should be compared with competitive parallel reaction of Villermaux/Dushman method based on iodide/iodate test reaction (Commence & Falk, 2011) to further benchmark the results. A meaningful comparison of the results obtained from these methods can be evaluated at varying operating conditions.

Microfluidics micromixers have been fabricated using different substrates, such as PDMS, PMMA, epoxy resin and glass. A comparative study investigating the effect of different substrates on mixing performance is proposed. This is because hydrophobicity or hydrophilicity property and surface roughness could influence the mixing performance.

Experimental components and methods used in this thesis can be used in specific area of study, for example in wastewater treatment or analysis. The proposed mixing index quantification method and the fabricated syringe pump could be an integral part of wastewater analysis, utilizing either active or passive micromixers.

REFERENCES

- Ansari, M. A., Kim, K.-Y., Anwar, K., & Kim, S. M. (2010). A novel passive micromixer based on unbalanced splits and collisions of fluid streams. *Journal of Micromechanics and Microengineering*, 20(5), 55007-55018.
- Ávila, M., Floris, A., Staal, S., Ríos, Á., Eijkel, J., & van den Berg, A. (2013). Point of care creatinine measurement for diagnosis of renal disease using a disposable microchip. *Electrophoresis*, 34(20-21), 2956-2961.
- Capretto, L., Cheng, W., Hill, M., & Zhang, X. (2011). Micromixing within microfluidic devices. In *Microfluidics* (pp. 27-68): Springer.
- Çengel, Y. A., & Cimbala, J. M. (2019). Fluid Mechanics: Fundamentals and Applications, 4e in SI Units. In: McGraw-Hill Education.
- Chen, C.-Y., Hsu, C.-C., Mani, K., & Panigrahi, B. (2016a). Hydrodynamic influences of artificial cilia beating behaviors on micromixing. *Chemical Engineering Processing: Process Intensification*, 99, 33-40.
- Chen, X., Li, T., Zeng, H., Hu, Z., & Fu, B. (2016b). Numerical and experimental investigation on micromixers with serpentine microchannels. *International Journal of Heat and Mass Transfer*, 98, 131-140.
- Chen, X., Shen, J., & Hu, Z. (2018). Fabrication and performance evaluation of two multi-layer passive micromixers. *Sensor Review*, 38(3), 321-325.
- Chen, X., Shen, J., & Zhou, M. (2016c). Rapid fabrication of a four-layer PMMA-based microfluidic chip using CO₂-laser micromachining and thermal bonding. *Journal of Micromechanics and Microengineering*, 26(10), 107001-107007.

- Chen, X., & Wang, X. (2015). Optimized modular design and experiment for staggered herringbone chaotic micromixer. *International Journal of Chemical Reactor Engineering*, 13(3), 305-309.
- Chen, X., & Zhao, Z. (2017). Numerical investigation on layout optimization of obstacles in a three-dimensional passive micromixer. *Analytica Chimica Acta*, 964, 142-149.
- Cheng, Z., Gu, Y., Li, S., Wang, Y., Chen, H., Cheng, J., & Liu, P. (2017). Enclosed casting of epoxy resin for rapid fabrication of rigid microfluidic chips. *Sensors and Actuators B: Chemical*, 252, 785-793.
- Commence, J.-M., & Falk, L. (2011). Villermaux–Dushman protocol for experimental characterization of micromixers. *Journal of Chemical Engineering Processing: Process Intensification*, 50(10), 979-990.
- Cortezzi, L., Ferrari, S., & Dubini, G. (2017). A scalable active micro-mixer for biomedical applications. *Microfluidics and Nanofluidics*, 21(3), 31-47.
- De Tarso Garcia, P., Cardoso, T. M. G., Garcia, C. D., Carrilho, E., & Coltro, W. K. T. (2014). A handheld stamping process to fabricate microfluidic paper-based analytical devices with chemically modified surface for clinical assays. *Rsc Advances*, 4(71), 37637-37644.
- Di Carlo, D. (2009). Inertial microfluidics. *Lab on a Chip*, 9(21), 3038-3046.
- Ding, S., Anton, N., Vandamme, T. F., & Serra, C. A. (2016). Microfluidic nanoprecipitation systems for preparing pure drug or polymeric drug loaded nanoparticles: an overview. *Expert Opinion on Drug Delivery*, 13(10), 1447-1460.
- Duarte-Guevara, P., Duarte-Guevara, C., Ornob, A., & Bashir, R. (2016). On-chip PMA labeling of foodborne pathogenic bacteria for viable qPCR and qLAMP detection. *Microfluidics and Nanofluidics*, 20(8), 114-113.

- Engler, M., Kockmann, N., Kiefer, T., & Woias, P. (2004). Numerical and experimental investigations on liquid mixing in static micromixers. *Chemical Engineering Journal*, *101*(1-3), 315-322.
- Evans, E., Gabriel, E. F. M., Benavidez, T. E., Coltro, W. K. T., & Garcia, C. D. (2014). Modification of microfluidic paper-based devices with silica nanoparticles. *Analyst*, *139*(21), 5560-5567.
- Faryadi, M., Rahimi, M., Safari, S., & Moradi, N. (2014). Effect of high frequency ultrasound on micromixing efficiency in microchannels. *Chemical Engineering and Processing: Process Intensification*, *77*, 13-21.
- Fu, H., Liu, X., & Li, S. (2017). Mixing indexes considering the combination of mean and dispersion information from intensity images for the performance estimation of micromixing. *RSC Advances*, *7*(18), 10906-10914.
- Galletti, C., Roudgar, M., Brunazzi, E., & Mauri, R. (2012). Effect of inlet conditions on the engulfment pattern in a T-shaped micro-mixer. *Chemical Engineering Journal*, *185*, 300-313.
- Gao, Z., Han, J., Bao, Y., & Li, Z. (2015). Micromixing efficiency in a T-shaped confined impinging jet reactor. *Chinese Journal of Chemical Engineering*, *23*(2), 350-355.
- Goda, K., Ayazi, A., Gossett, D. R., Sadasivam, J., Lonappan, C. K., Sollier, E., . . . Murray, C. (2012). High-throughput single-microparticle imaging flow analyzer. *Proceedings of the National Academy of Sciences*, *109*(29), 11630-11635.
- Heshmatnezhad, F., Aghaei, H., & Nazar, A. R. S. (2017). Parametric Study of Obstacle Geometry Effect on Mixing Performance in a Convergent-Divergent Micromixer with Sinusoidal Walls. *Chemical Product Process Modeling*, *12*(1), 1-12.

- Hong, C.-C., Choi, J.-W., & Ahn, C. H. (2004). A novel in-plane passive microfluidic mixer with modified Tesla structures. *Lab on a Chip*, 4(2), 109-113.
- Hong, T.-F., Ju, W.-J., Wu, M.-C., Tai, C.-H., Tsai, C.-H., & Fu, L.-M. (2010). Rapid prototyping of PMMA microfluidic chips utilizing a CO₂ laser. *Microfluidics and Nanofluidics*, 9(6), 1125-1133.
- Hou, X., Zhang, Y. S., Trujillo-de Santiago, G., Alvarez, M. M., Ribas, J., Jonas, S. J., . . . Khademhosseini, A. (2017). Interplay between materials and microfluidics. *Nature Reviews Materials*, 2(5), 1-15.
- ITU (Producer). (2011). RECOMMENDATION ITU-R BT.601-5 :Studio encoding parameters of digital television for standard 4: 3 and wide-screen 16: 9 aspect ratios. Retrieved from <https://www.itu.int/rec/R-REC-BT.601/>
- Jafarian, A., Pishavar, A., & Saidi, M. (2014). Modeling active micromixers with multiple microstirrers using smoothed particle hydrodynamics. *Scientia Iranica. Transaction B, Mechanical Engineering*, 21(4), 1390-1402.
- Jännig, O., & Nguyen, N.-T. (2011). A polymeric high-throughput pressure-driven micromixer using a nanoporous membrane. *Microfluidics and Nanofluidics*, 10(3), 513-519.
- Jeon, N. L., Dertinger, S. K., Chiu, D. T., Choi, I. S., Stroock, A. D., & Whitesides, G. M. (2000). Generation of solution and surface gradients using microfluidic systems. *Langmuir*, 16(22), 8311-8316.
- Jia, X., Wang, W., Han, Q., Wang, Z., Jia, Y., & Hu, Z. (2016). Micromixer based preparation of functionalized liposomes and targeting drug delivery. *ACS Medicinal Chemistry Letters*, 7(4), 429-434.

- Jiang, F., Drese, K. S., Hardt, S., Küpper, M., & Schönfeld, F. (2004). Helical flows and chaotic mixing in curved micro channels. *American Institute of Chemical Engineers Journal*, 50(9), 2297-2305.
- Jiang, L., Wang, W., Chau, Y., & Yao, S. (2013). Controllable formation of aromatic nanoparticles in a three-dimensional hydrodynamic flow focusing microfluidic device. *RSC Advances*, 3(39), 17762-17769.
- Joanni, E., Peressinotto, J., Domingues, P. S., de Oliveira Setti, G., & de Jesus, D. P. (2015). Fabrication of molds for PDMS microfluidic devices by laser swelling of PMMA. *RSC Advances*, 5(32), 25089-25096.
- Johnson, T. J., Ross, D., & Locascio, L. E. (2002). Rapid microfluidic mixing. *Analytical Chemistry*, 74(1), 45-51.
- Karthikeyan, K., & Sujatha, L. (2019). Study of Permissible Flow Rate and Mixing Efficiency of the Micromixer Devices. *International Journal of Chemical Reactor Engineering*, 17(1), 1-15.
- Kastner, E., Verma, V., Lowry, D., & Perrie, Y. (2015). Microfluidic-controlled manufacture of liposomes for the solubilisation of a poorly water soluble drug. *International Journal of Pharmaceutics*, 485(1-2), 122-130.
- Khozeymeh-Nezhad, H., & Niazmand, H. (2018). A double MRT-LBM for simulation of mixing in an active micromixer with rotationally oscillating stirrer in high Peclet number flows. *International Journal of Heat and Mass Transfer*, 122, 913-921.
- Kim, H.-S., Kim, H.-O., & Kim, Y.-J. (2018). *Effect of Electrode Configurations on the Performance of Electro-Hydrodynamic Micromixer*. Paper presented at the ASME 2018 16th International Conference on Nanochannels, Microchannels, and Minichannels.

- Kim, J., Taylor, D., Agrawal, N., Wang, H., Kim, H., Han, A., . . . Jayaraman, A. (2012). A programmable microfluidic cell array for combinatorial drug screening. *Lab on a Chip*, 12(10), 1813-1822.
- Kim, S.-J., Wang, F., Burns, M. A., & Kurabayashi, K. (2009). Temperature-programmed natural convection for micromixing and biochemical reaction in a single microfluidic chamber. *Analytical Chemistry*, 81(11), 4510-4516.
- Kumar, V., Paraschivoiu, M., & Nigam, K. (2011). Single-phase fluid flow and mixing in microchannels. *Chemical Engineering Science*, 66(7), 1329-1373.
- Kwak, T. J., Nam, Y. G., Najera, M. A., Lee, S. W., Strickler, J. R., & Chang, W.-J. (2016). Convex grooves in staggered herringbone mixer improve mixing efficiency of laminar flow in microchannel. *PloS One*, 11(11), 1-15.
- Le The, H., Le Thanh, H., Dong, T., Ta, B. Q., Tran-Minh, N., & Karlsen, F. (2015). An effective passive micromixer with shifted trapezoidal blades using wide Reynolds number range. *Chemical Engineering and Research Design*, 93, 1-11.
- Lee, C.-Y., & Fu, L.-M. (2018). Recent advances and applications of micromixers. *Sensors and Actuators B: Chemical*, 259, 677-702.
- Lee, C.-Y., Wang, W.-T., Liu, C.-C., & Fu, L.-M. (2016). Passive mixers in microfluidic systems: A review. *Chemical Engineering Journal*, 288, 146-160.
- Li, Y., Zhang, D., Feng, X., Xu, Y., & Liu, B.-F. (2012). A microsecond microfluidic mixer for characterizing fast biochemical reactions. *Talanta*, 88, 175-180.
- Lin, C.-H., Fu, L.-M., & Chien, Y.-S. (2004). Microfluidic T-form mixer utilizing switching electroosmotic flow. *Analytical Chemistry*, 76(18), 5265-5272.
- Lin, M. X., Hyun, K.-A., Moon, H.-S., Sim, T. S., Lee, J.-G., Park, J. C., . . . Jung, H.-I. (2013). Continuous labeling of circulating tumor cells with microbeads using a

- vortex micromixer for highly selective isolation. *Biosensors and Bioelectronics*, 40(1), 63-67.
- Liu, G., Ma, X., Wang, C., Sun, X., & Tang, C. (2018). Piezoelectric driven self-circulation micromixer with high frequency vibration. *Journal of Micromechanics and Microengineering*, 28(8), 1-12.
- Lu, M., Ozcelik, A., Grigsby, C. L., Zhao, Y., Guo, F., Leong, K. W., & Huang, T. J. (2016). Microfluidic hydrodynamic focusing for synthesis of nanomaterials. *Nano Today*, 11(6), 778-792.
- Luo, P., Cheng, Y., Wang, Z., Jin, Y., & Yang, W. (2006). Study on the mixing behavior of thin liquid-sheet impinging jets using the PLIF technique. *Industrial Engineering Chemistry Research*, 45(2), 863-870.
- Mäki, A.-J., Hemmilä, S., Hirvonen, J., Girish, N. N., Kreutzer, J., Hyttinen, J., & Kallio, P. (2015). Modeling and experimental characterization of pressure drop in gravity-driven microfluidic systems. *Journal of Fluids Engineering*, 137(2), 1-8.
- Matsunaga, T., Lee, H.-J., & Nishino, K. (2013). An approach for accurate simulation of liquid mixing in a T-shaped micromixer. *Lab on a Chip*, 13(8), 1515-1521.
- McDonough, J., Oates, M., Law, R., & Harvey, A. (2019). Micromixing in oscillatory baffled flows. *Chemical Engineering Journal*, 361, 508-518.
- Mukhopadhyay, S. (2017). Experimental investigations on the interactions between liquids and structures to passively control the surface-driven capillary flow in microfluidic lab-on-a-chip systems to separate the microparticles for bioengineering applications. *Surface Review and Letters*, 24(06), 1-10.

- Nimafar, M., Viktorov, V., & Martinelli, M. (2012). Experimental comparative mixing performance of passive micromixers with H-shaped sub-channels. *Chemical Engineering Science*, 76, 37-44.
- Nouri, D., Zabihi-Hesari, A., & Passandideh-Fard, M. (2017). Rapid mixing in micromixers using magnetic field. *Sensors and Actuators A: Physical*, 255, 79-86.
- Ogilvie, I., Sieben, V., Floquet, C., Zmijan, R., Mowlem, M., & Morgan, H. (2010). Reduction of surface roughness for optical quality microfluidic devices in PMMA and COC. *Journal of Micromechanics and Microengineering*, 20(6), 1-8.
- Park, J.-Y., Kim, Y.-D., Kim, S.-R., Han, S.-Y., & Maeng, J.-S. (2008). Robust design of an active micro-mixer based on the Taguchi method. *Sensors and Actuators B: Chemical*, 129(2), 790-798.
- Parsa, M. K., Hormozi, F., & Jafari, D. (2014). Mixing enhancement in a passive micromixer with convergent–divergent sinusoidal microchannels and different ratio of amplitude to wave length. *Computers and Fluids*, 105, 82-90.
- Parvizian, F., Rahimi, M., & Faryadi, M. (2011). Macro-and micromixing in a novel sonochemical reactor using high frequency ultrasound. *Chemical Engineering Processing: Process Intensification*, 50(8), 732-740.
- Prakash, S., & Kumar, S. (2015). Fabrication of microchannels on transparent PMMA using CO₂ Laser (10.6 μm) for microfluidic applications: An experimental investigation. *International Journal of Precision Engineering and Manufacturing*, 16(2), 361-366.
- Rafeie, M., Welleweerd, M., Hassanzadeh-Barforoushi, A., Asadnia, M., Olthuis, W., & Ebrahimi Warkiani, M. (2017). An easily fabricated three-dimensional threaded lemniscate-shaped micromixer for a wide range of flow rates. *Biomicrofluidics*, 11(1), 1-15.

- Rahimi, M., Azimi, N., & Parvizian, F. (2013). Using microparticles to enhance micromixing in a high frequency continuous flow sonoreactor. *Chemical Engineering and Processing: Process Intensification*, 70, 250-258.
- Rapp, B. E. (2016). *Microfluidics: Modeling, Mechanics and Mathematics*: William Andrew.
- Rudyak, V., & Minakov, A. (2014). Modeling and optimization of Y-type micromixers. *Micromachines*, 5(4), 886-912.
- Ryu, S.-P., Park, J.-Y., & Han, S.-Y. (2011). Optimum design of an active micro-mixer using successive Kriging method. *International Journal of Precision Engineering and Manufacturing*, 12(5), 849-855.
- Sakurai, R., Yamamoto, K., & Motosuke, M. (2018). Concentration-adjustable micromixer using droplet injection into a microchannel. *Analyst*, 144, 2780-2787.
- Sarkar, S., Singh, K., Shankar, V., & Shenoy, K. (2014). Numerical simulation of mixing at 1–1 and 1–2 microfluidic junctions. *Chemical Engineering and Processing: Process Intensification*, 85, 227-240.
- Sasaki, N., Kitamori, T., & Kim, H.-B. (2006). AC electroosmotic micromixer for chemical processing in a microchannel. *Lab on a Chip*, 6(4), 550-554.
- Sayad, A. A., Ibrahim, F., Uddin, S. M., Pei, K. X., Mohktar, M. S., Madou, M., & Thong, K. L. (2016). A microfluidic lab-on-a-disc integrated loop mediated isothermal amplification for foodborne pathogen detection. *Sensor and Actuators B: Chemical*, 227, 600-609.
- Scherr, T., Quitadamo, C., Tesvich, P., Park, D. S.-W., Tiersch, T., Hayes, D., . . . Monroe, W. T. (2012). A planar microfluidic mixer based on logarithmic spirals. *Journal of Micromechanics and Microengineering*, 22(5), 1-10.

- Seip, R., & Ebbini, E. S. (1995). Noninvasive estimation of tissue temperature response to heating fields using diagnostic ultrasound. *IEEE Transactions on Biomedical Engineering*, 42(8), 828-839.
- Shah, I., Kim, S. W., Kim, K., Doh, Y. H., & Choi, K. H. (2019). Experimental and numerical analysis of Y-shaped split and recombination micro-mixer with different mixing units. *Chemical Engineering Journal*, 358, 691-706.
- Shamloo, A., Vatankhah, P., & Akbari, A. (2017). Analyzing mixing quality in a curved centrifugal micromixer through numerical simulation. *Chemical Engineering and Processing: Process Intensification*, 116, 9-16.
- Shamsoddini, R. (2018). SPH investigation of the thermal effects on the fluid mixing in a microchannel with rotating stirrers. *Fluid Dynamics Research*, 50(2), 1-17.
- Shamsoddini, R., Sefid, M., & Fatehi, R. (2016). Incompressible SPH modeling and analysis of non-Newtonian power-law fluids, mixing in a microchannel with an oscillating stirrer. *Journal of Mechanical Science and Technology*, 30(1), 307-316.
- Sivashankar, S., Agambayev, S., Mashraei, Y., Li, E. Q., Thoroddsen, S. T., & Salama, K. N. (2016). A “twisted” microfluidic mixer suitable for a wide range of flow rate applications. *Biomicrofluidics*, 10(3), 1- 13.
- Sudarsan, A. P., & Ugaz, V. M. (2006). Fluid mixing in planar spiral microchannels. *Lab on a Chip*, 6(1), 74-82.
- Surdo, S., Diaspro, A., & Duocastella, M. (2017). Micromixing with spark-generated cavitation bubbles. *Microfluidics and Nanofluidics*, 21(5), 82-93.
- Sutkar, V. S., & Gogate, P. R. (2010). Mapping of cavitation activity in high frequency sonochemical reactor. *Chemical Engineering Journal*, 158(2), 296-304.

- Ta, B. Q., Lê Thanh, H., Dong, T., Thoi, T. N., & Karlsen, F. (2015). Geometric effects on mixing performance in a novel passive micromixer with trapezoidal-zigzag channels. *Journal of Micromechanics and Microengineering*, 25(9), 1-11.
- Walker, G. M., & Beebe, D. J. (2002). A passive pumping method for microfluidic devices. *Lab on a Chip*, 2(3), 131-134.
- Wang, H., Shi, L., Zhou, T., Xu, C., & Deng, Y. (2018). A novel passive micromixer with modified asymmetric lateral wall structures. *Asia-Pacific Journal of Chemical Engineering*, 13(3), 1-11.
- Wang, L., Liu, D., Wang, X., & Han, X. (2012). Mixing enhancement of novel passive microfluidic mixers with cylindrical grooves. *Chemical Engineering Science*, 81, 157-163.
- Wang, Z., Han, T., Jeon, T.-J., Park, S., & Kim, S. M. (2013). Rapid detection and quantification of bacteria using an integrated micro/nanofluidic device. *Sensors and Actuators B:Chemical*, 178, 683-688.
- Ward, K., & Fan, Z. H. (2015). Mixing in microfluidic devices and enhancement methods. *Journal of Micromechanics Microengineering*, 25(9), 1-17.
- Witkowski, D., Kubicki, W., Dziuban, J. A., Jašíková, D., & Karczemska, A. (2018). Micro-Particle Image Velocimetry for imaging flows in passive microfluidic mixers. *Metrology and Measurement Systems*, 25(3), 441-450.
- World Health Organization. (2018). Diabetes. Retrieved from <https://www.who.int/news-room/fact-sheets/detail/diabetes>
- Wu, J., Dong, M., Rigatto, C., Liu, Y., & Lin, F. (2018). Lab-on-chip technology for chronic disease diagnosis. *NPJ Digital Medicine*, 1(1), 1-7.

- Xu, B., Wong, T. N., & Nguyen, N.-T. (2011). Experimental and numerical investigation of thermal chaotic mixing in a T-shaped microchannel. *Heat and Mass Transfer*, 47(11), 1331-1339.
- Xu, C., & Chu, Y. (2015). Experimental study on oscillating feedback micromixer for miscible liquids using the Coanda effect. *American Institute of Chemical Engineers Journal*, 61(3), 1054-1063.
- Yamamoto, D., Maki, T., Watanabe, S., Tanaka, H., Miyahara, M. T., & Mae, K. (2013). Synthesis and adsorption properties of ZIF-8 nanoparticles using a micromixer. *Chemical Engineering Journal*, 227, 145-150.
- Yang, J.-T., Huang, K.-J., Tung, K.-Y., Hu, I.-C., & Lyu, P.-C. (2007). A chaotic micromixer modulated by constructive vortex agitation. *Journal of Micromechanics and Microengineering*, 17(10), 2084-2092.
- Yang, Z., Matsumoto, S., Goto, H., Matsumoto, M., & Maeda, R. (2001). Ultrasonic micromixer for microfluidic systems. *Sensors and Actuators A: Physical*, 93(3), 266-272.
- Yap, Y. C., Guijt, R. M., Dickson, T. C., King, A. E., & Breadmore, M. C. (2013). Stainless steel pinholes for fast fabrication of high-performance microchip electrophoresis devices by CO₂ laser ablation. *Analytical Chemistry*, 85(21), 10051-10056.
- Yaralioglu, G. G., Wygant, I. O., Marentis, T. C., & Khuri-Yakub, B. T. (2004). Ultrasonic mixing in microfluidic channels using integrated transducers. *Analytical Chemistry*, 76(13), 3694-3698.
- You, J. B., Kang, K., Tran, T. T., Park, H., Hwang, W. R., Kim, J. M., & Im, S. G. (2015). PDMS-based turbulent microfluidic mixer. *Lab on a Chip*, 15(7), 1727-1735.

Zha, L., Pu, X., Shang, M., Li, G., Xu, W., Lu, Q., & Su, Y. (2018). A study on the micromixing performance in microreactors for polymer solutions. *American Institute of Chemical Engineers Journal*, 64(9), 3479-3490.

APPENDICES

Journal Publications

1. **Mahmud, F.,** & Tamrin, K. F. (2020). Method for determining mixing index in microfluidics by RGB color model. *Asia-Pacific Journal of Chemical Engineering*, 15(2), e2407.
2. **Mahmud, F.,** Tamrin, K., & Sheikh, N. (2020). A Review of Enhanced Micromixing Techniques in Microfluidics for the Application in Wastewater Analysis. In *Advances in Waste Processing Technology* (pp. 1-22): Springer.